CHAPTER III

RESULTS AND DISCUSSION

In this chapter, the results of X-radiography and time series measurements of stable isotopes, radiocarbon and Cd made in various corals are presented and discussed. For clarity the chapter is divided into five sections.

The first section is on X-radiography and growth rates of corals. The second section deals with the results of stable isotope (O and C) data and their interpretation. Section three focuses on the determination of the air-sea carbon-dioxide exchange rate in the Gulf of Kutch based on radiocarbon analyses of coral bands and tree rings. Cadmium measurements are presented in the fourth section. The last section deals with the intercomparison and synthesis of the results of different corals analyzed.

III.1 X-RADIOGRAPHIC ANALYSIS

X-radiography is a useful tool to obtain information on banding in corals and their growth rates. In the previous chapter we had mentioned in some detail the methodology used by us for mapping coral banding using X-ray photography. Here we present the results.

The first coral we analyzed was a *Porites compressa* (KV-1) from Lakshadweep region (LDP). It showed 5 bands with alternate high and low density growth rings, corresponding to dark and light colour respectively in the X-ray positive. From this X-ray picture we determined the average band width (made of one dark and the adjoining light band) as 23.3±1.9 mm. Oxygen isotope studies of this coral (discussed in the next section) showed that the bands are annual in nature. Such a high growth rate enabled us to subsample the bands with a resolution better than a fortnight for stable isotopic studies (average of 28 samples per band). Another *P. compressa* (Am) from the Amini island also showed 4 bands with an average thickness of 22.5±3.7 mm. In this coral, for stable

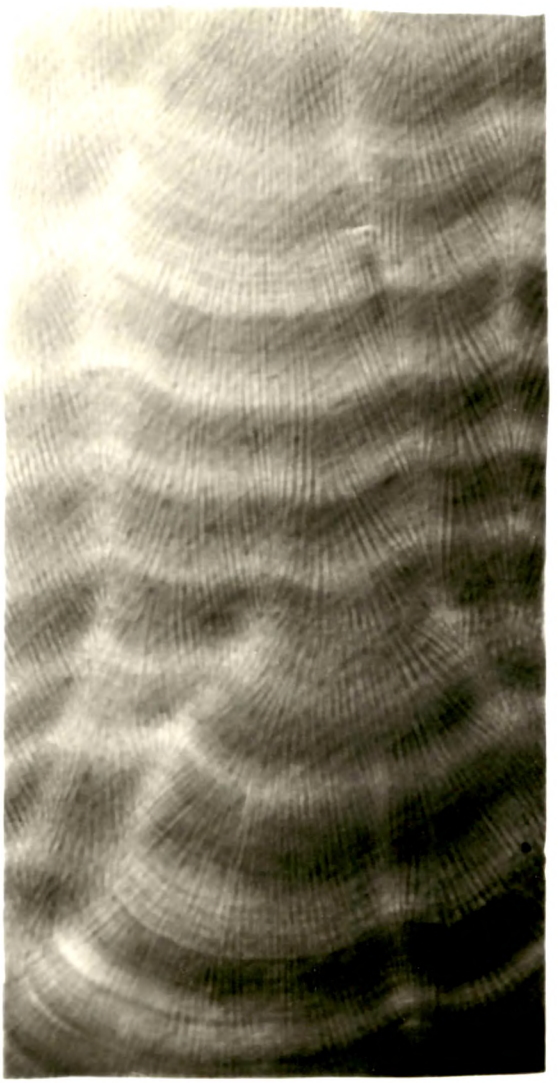

Fig 3.1 X-radiograph of the coral *Porites compressa* (KV-2) collected from Kavaratti lagoon, Lakshadweep islands. The average bandwidth of this coral is 15 ± 3.4 mm.

isotopic measurements 9 samples per band were taken. The coral KV-2, also a *Porites compressa* from Kavaratti atoll on which extensive oxygen and carbon isotope measurements were made, showed 25 growth bands corresponding to 25 years of age. Its average growth rate was 15±3.4 mm/yr. Fig 3.1 shows a portion of the X-ray positive of this coral. This coral was sampled for stable isotopic studies with a resolution of 8 to 16 samples per band. The sample (GK) from the Gulf of Kutch, a *Favia speciosa*, had 40 growth bands. The mean band thickness of this coral was only 4.3±1.3 mm. Because of the smaller band width, the time resolution for isotopic studies in this coral was poorer compared to that of Lakshadweep corals. About 2 to 5 samples per band were analyzed. The sample (SR), a *Porites lutea* collected from the Stanley Reef of Great Barrier Reef, Australia (by Dr J M Lough) had 20 bands, with an average band width of 11.7±3 mm. Two tracks were chosen for isotopic and densitometric analyses. One close to growth axis (10° off), other ~20° off the growth axis. Fig 3.2 shows the variations of bandwidth in KV-2, GK and SR corals respectively. Also shown in this figure (inset) are the bandwidth variations of KV-1 and Am corals. Table 3.1 gives a summary of the bandwidth measurements. All the samples mentioned above formed a single band in a year. This was revealed by oxygen isotopic analysis presented in the following section; hence the bands represent annual skeletal extensions.

The species identification of Lakshadweep corals was done by Dr M V M Wafar of National Institute of Oceanography, Goa and Mr M I Patel of Gujarat State Fisheries Aquatic Sciences Research Station, Sikka, Gujarat and that of the Gulf of Kutch and Stanley Reef corals by Dr J Veron of Australian Institute of Marine Science, Townsville, Australia.

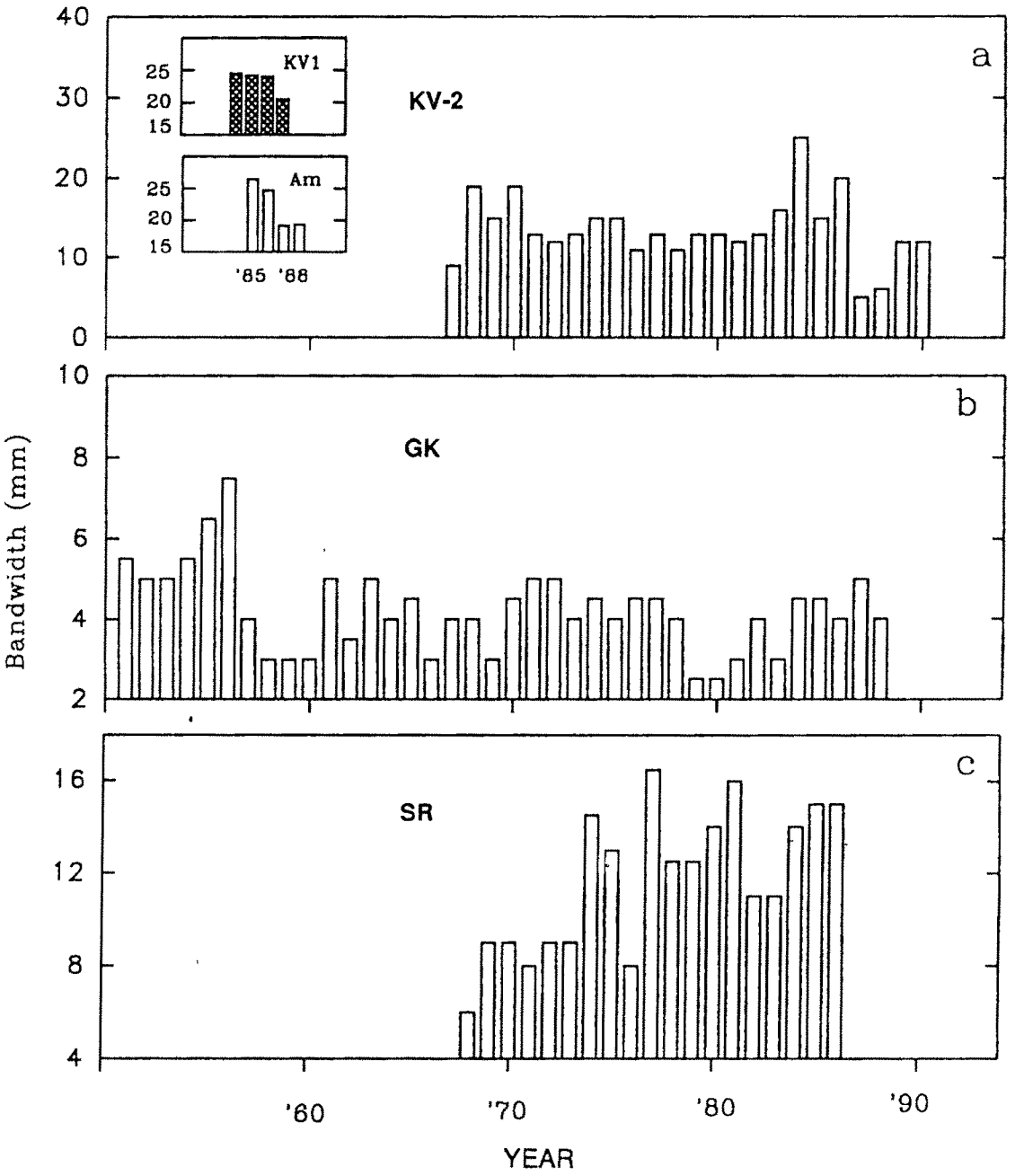

Fig 3.2 Variations in bandwidth with time in corals from (a) Kavaratti (Lakshadweep): (KV-2), (b) Gulf of Kutch, (GK) and (c) Stanley Reef, (SR) region. The insets in box a are for two younger corals from Kavaratti (KV-1) and Amini (Am) from the Lakshadweep. X-axis is not a calender year but the year corresponding to one high + one low density band.

Table III.1 Range and mean bandwidths of various coral samples used in this work

Coral code	No. of bands	Bandwidth(mm)	
		Range	Mean±1σ
KV-1	5	20.5-24.5	23.3±1.9
Am	4	19.2-26.5	22.5±3.7
KV-2	25	10-23	15±3.4
GK	41	2.5-7.5	4.3±1.3
SR	19	6-16.5	11.7±3

The variations in bandwidth or rates of coral growth which vary among the coral genera are controlled by various environmental parameters. The corals from Lakshadweep have higher growth rates compared to the Gulf of Kutch coral, possibly because Lakshadweep region has light and temperature conditions more suited for coral growth.

III.2 STABLE ISOTOPIC STUDIES

As mentioned in the last chapter stable oxygen and carbon isotope measurements were made on corals from the Lakshadweep, the Gulf of Kutch and the Stanley Reef. The results are presented regionwise below.

III.2.a Lakshadweep corals

Stable isotopic measurements were made on three corals from the Lakshadweep islands; KV-1 & KV-2 from the Kavaratti island, Am and a giant clam (GC) from the Amini island.

The first sample analyzed was KV-1, a five year old *Porites*. This coral had an average bandwidth of 2.3 cm based on X-radiography (Table III.1). Oxygen and carbon isotope measurements were made on an average of about 28 samples per band. This

provided a time resolution of better than a fortnight per sample. The seasonal chronology was assigned to the $\delta^{18}O$ profile of this coral using SST and $\delta^{18}O$ of water. This was subsequently followed for all other *P. compressa* corals from this region. The results of Am and GC were used to quantify the disequilibrium offset (in $\delta^{18}O$) and to standardize coral thermometry for retrieving SST of this region. The resulting equation was then applied to the $\delta^{18}O$ signatures on the longer lived coral KV-2 to derive SST for the last seventeen years and compare the results with the instrumental records.

Time variations in $\delta^{13}C$ and $\delta^{18}O$ of the coral KV-1 are shown in Fig 3.3. Table-III.2 and III.3 in the Appendix-A list these data.

(i) *Oxygen isotopes*

The $\delta^{18}O$ of this coral ranges from -5.6 to -4.8‰ (Fig 3.3). The seasonal changes in $\delta^{18}O$ in coral $CaCO_3$ are influenced both by SST and $\delta^{18}O$ of water. To evaluate how in this region SST and $\delta^{18}O$ of water control the $\delta^{18}O$ of the coral $CaCO_3$ we approach as follows. The monthly average values of SST are shown in Fig 3.4a. These are based on the COADS (Comprehensive Ocean Atmosphere Data Set) SST data for a location near to Kavaratti (10°N, 74°E, 2°×2° grid) for the period of 1974 to 1980 A.D. Data on the $\delta^{18}O$ of water are not available for this region. Therefore we have derived the $\delta^{18}O$ of water based on salinity. The available results (Duplessey *et al.* 1981) along the west coast of India, show that for every 1‰ increase in salinity, the $\delta^{18}O$ of sea water increases by about 0.3‰ (used by Sarkar *et al.* 1990). Assuming that this relationship also holds for the Lakshadweep region, we have derived the $\delta^{18}O$ of the water, using the salinity data from the bimonthly averages given in the Oceanographic Atlas (Wyrtki 1971), the values for the sample location were obtained by reading between contours (0.5‰). The calculated $\delta^{18}O$ values for the waters are given in Fig 3.4b (In order to check the assumption on the salinity-$\delta^{18}O$ relation mentioned above, we analyzed water samples collected from the Kavaratti lagoon during Apr 1988 and Dec 1988. The salinity difference between these two periods is 1‰. The observed $\delta^{18}O$ difference is 0.3±0.3‰). The quoted error is not experimental uncertainties but sample to sample variability. We have analyzed a total of 7 samples for April and 12 samples for December.

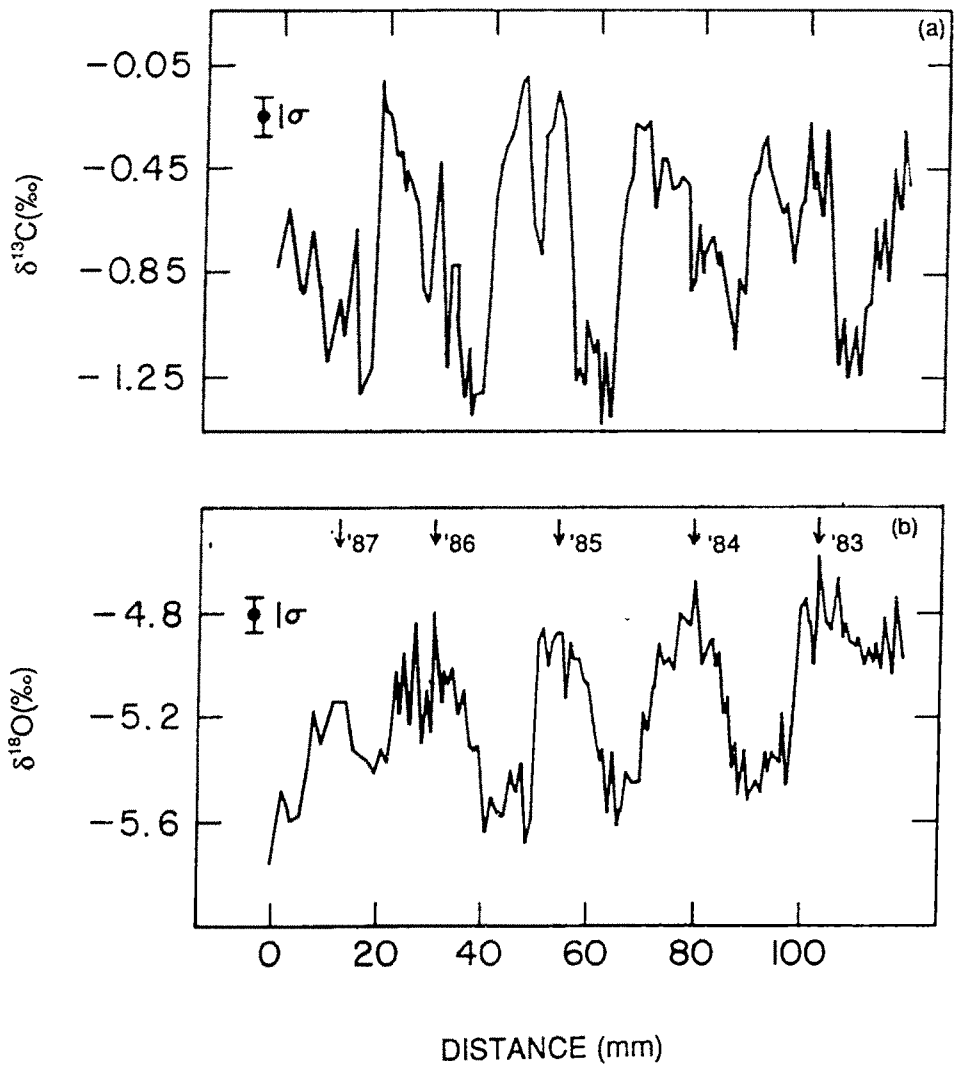

Fig 3.3 $\delta^{13}C$ (a) and $\delta^{18}O$ (b) variations in the *Porites compressa* (KV-1) from the Kavaratti lagoon, Lakshadweep Is. Distance is measured inward, from the coral surface (live when collected) to its base. August of each year is marked by an arrow.

Based on the SST and $\delta^{18}O$ of sea water (relative to PDB) during the course of the year, we can derive the $\delta^{18}O$ in coralline $CaCO_3$ (for calculation a temperature coefficient of -0.2‰ per °C is used). From Oct to Feb, the temperature is more or less constant at about 28°C (within one standard deviation, which represents the interannual SST variability). During this period the $\delta^{18}O$ of seawater decreases by about 0.3‰, causing a decrease of 0.3‰ in the $\delta^{18}O$ of coral. From Feb to Apr, there is a steady increase in the SST by about 2°C, whereas the $\delta^{18}O$ of water remains constant at around 0.15‰. For this period we would expect the $\delta^{18}O$ of coral $CaCO_3$ to decrease by 0.4‰. From May to Aug, due to monsoon induced upwelling, there is a reduction in SST by about 3°C, and an increase in $\delta^{18}O$ of water by about 0.3‰. The reduction in SST and increase in salinity both favour increase in $\delta^{18}O$ of coral $CaCO_3$. Therefore during this period, the coral $\delta^{18}O$ increases by 0.9‰. From Aug to Oct the SST increases by 1°C and the $\delta^{18}O$ of water decreases by 0.15‰. Both these changes together cause a reduction in coral $\delta^{18}O$ by about 0.35‰.

Summing up, the pattern of variations of SST and $\delta^{18}O$ of water should be reflected in the $\delta^{18}O$ of coral $CaCO_3$ by a minimum around Apr-May and maximum during Aug. The expected coral $\delta^{18}O$ (seasonal) variation is (~ 0.9‰) as shown in Fig 3.4c. With this information it is possible to assign specific time slots (in terms of months) to the $\delta^{18}O$ data shown in Fig 3.3b. The minimum value (-5.6‰) in $\delta^{18}O$ corresponds to Apr-May while the maximum value (~ -4.8‰) corresponds to Aug. The monsoon induced cooling is manifested as an increase in the $\delta^{18}O$ value from about -5.6‰ to -4.8‰, the range being 0.8‰ similar to the expected value of 0.9‰.

To translate the $\delta^{18}O$ time series in the coral $CaCO_3$ to SST it is necessary to quantitatively assess the isotopic disequilibrium offset since corals do not precipitate $CaCO_3$ in isotopic equilibrium (Weber 1974, Weber & Woodhead 1972, Swart 1983). The complex biological processes, such as metabolism and endosymbiotic photosynthesis, result in metabolic and/or kinetic fractionation. These processes deplete the isotopic composition (*i.e.* ratio of heavy to light isotopes) of coral $CaCO_3$ relative to that expected for equilibrium precipitation. The deviation from the equilibrium precipitation can be represented by the following equation (Aharon 1991).

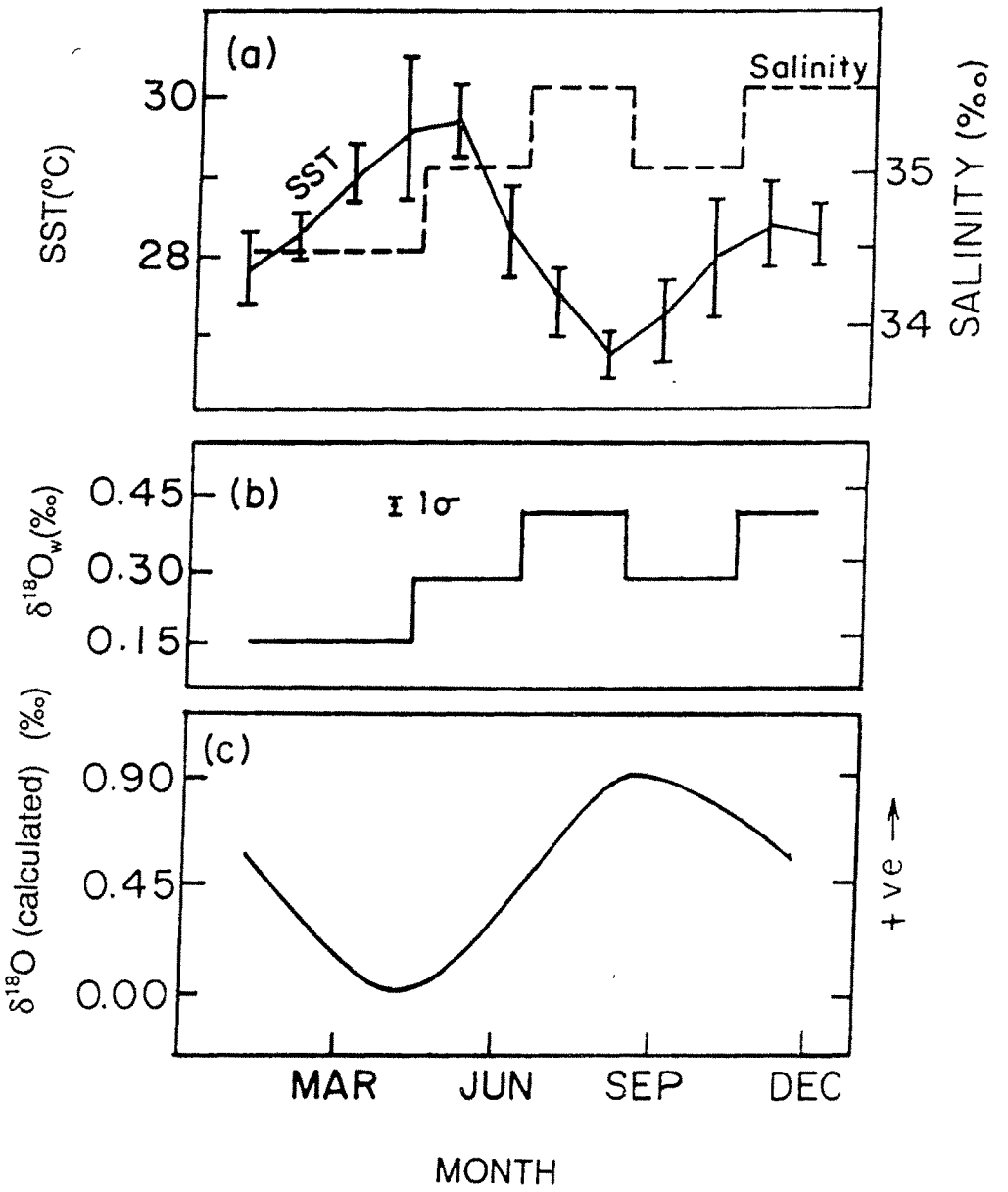

Fig 3.4(a) Mean monthly SST (solid line) and bimonthly averages of salinity (dotted line) for the region 10°N, 74°E. The error bars for SST show 1σ variations around the mean of 7 years. (b) $\delta^{18}O$ of water (relative to PDB) calculated from salinity data and $\delta^{18}O$-salinity relation for this region (Duplessey *et al.* 1981). (c) estimated $\delta^{18}O$ variations of coral based on SST and $\delta^{18}O$ of water. Y-axis represents a relative scale.

$$\delta^{18}O_{coral} = \delta^{18}O_{eq} + \delta^{18}O_{off} \quad (3.1)$$

where $\delta^{18}O_{off}$ is the "offset" term. This offset has so far been assumed to be constant with time, within the limits of experimental uncertainties for a given coral species. The offset from equilibrium value in symbiont bearing corals of Indo-Pacific origin ranges from -3.12 to -1.93‰ at 25°C among 44 coral genera analyzed by Weber & Woodhead (1972). Aharon (1991) obtained a value of -5.1‰ for *Porites* from the Palm Isles.

We determined the $\delta^{18}O_{off}$ for *Porites* of Lakshadweep by comparing $\delta^{18}O$ profiles in a coral (Am) from the Amini island with that in a giant clam (GC) that grew near the coral. It is known that the giant clam (*Tridacna*) precipitates its $CaCO_3$ in isotopic equilibrium (Aharon & Chappel 1986; Romanek & Grossman 1989), hence it is possible to correct for the coral $\delta^{18}O$ disequilibrium offset by comparing $\delta^{18}O$ values in time contemporaneous samples of coral and a bivalve.

We collected a live coral head (*Porites*) and a giant clam (*Tridacna maximus*) from the Amini island (11°7'N,72°44'E) in December 1988. Band assignment in the Amini coral was made following the procedure discussed earlier for the Kavaratti coral. This coral had a life span of about 5 years. In the case of *Tridacna*, year assignment was possible by identifying the annual zonation in the exoskeleton (Aharon & Chappel, 1986). $\delta^{18}O$ data for the clam and the Amini coral are given in Table III.2 (Appendix A). We have estimated the disequilibrium offset in the *P. compressa* coral by comparing the $\delta^{18}O$ values of the two during the life span of the coral, 1983-1988. Again, because of the difference in the growth rates, only the maxima, minima values of the two are compared. This yields a mean value of -4.47 ± 0.23‰ for the disequilibrium offset and ranges between -4.22 to -5.00‰. Note that all these disequilibrium factors are relative to aragonite equilibrium values. We consider our estimate of disequilibrium offset to be better than that available in literature (Aharon 1991) because the coral and the clam were growing very close to each other ~1m, compared to ~ 3km separation in earlier work. Our estimate of disequilibrium offset appears to be constant (within ±0.2‰) with time.

From the available data on SST, $\delta^{18}O$ of clam, and $\delta^{18}O$ of sea water for April and August we derive a regression line of the form:

$$T(°C) = A + B\ (\delta_c - \delta_w) \quad (3.2)$$

where δ_c and δ_w are the $\delta^{18}O$ of the clam and sea water wrt PDB respectively. For this,

we have taken the δ_w values to be 0.28 and 0.415 for May and August respectively (see Fig 3.4). This assumes that there is no year to year change in seasonal δ_w. This can cause some uncertainty in the accurate evaluation of SST from the coral $\delta^{18}O$. This is discussed later.

Fitting of our measured yearly maximum and minimum oxygen isotope data of the clam with corresponding SST (for 1983-1988) yields: A=23.92±0.35 and B=−4.68±0.33, with a correlation coefficient r=-0.92 significant at 0.01 level. Substituting these values in Eqn (3.2) we get,

$$T(°C) = 23.92 - 4.68\ (\delta_c - \delta_w) \qquad (3.3)$$

This is similar to the equation [$T = 20.95 - 4.35(\delta_c-\delta_w)$] obtained by Aharon & Chappel (1986) for tridacnid clams between temperatures of 23 to 28°C. The slopes of these two equations agree within analytical uncertainties, but the intercepts differ by 3°C. One possible explanation for this may be the difference in temperature ranges in the two localities. In Lakshadweep the maximum temperature exceeds 30°C in summer, occasionally it reaches even 35°C for a few days.

Substituting for δ_c in Eqn (3.3) in terms of δ_{coral} and the disequilibrium offset, we obtain the temperature equation for SST based on the coral $\delta^{18}O$.

$$T(°C) = 3.0 - 4.68(\delta_{coral} - \delta_w) \qquad (3.4)$$

where δ_{coral} is the $\delta^{18}O$ value of the *Porites* coral. This equation is quite similar to that reported for *Porites* from the Pacific (Aharon, 1991):

$$T = 2.81 - 4.76(\delta_{coral} - \delta_w) \qquad (3.5)$$

The slope is also in agreement with that for *Porites* from the Atlantic (Druffel 1985). The uncertainties in estimating temperature using Eqn (3.5) are: (i) there may be small changes from equilibrium values even for the tridacnid clams ranging from 0.1 to 0.3‰ (Aharon 1991); this would correspond to 0.5 to 1.5 °C difference in the estimated SSTs, (ii) the SST values used by us for deriving the temp-$\delta^{18}O$ equation (Eqn 3.4) are not from the exact location of the clam. This may cause an additional uncertainty.

The estimated uncertainty in SST based on Eqn 3.4 is calculated to be 1.4°C considering the errors in δ_w (0.2‰) and that in the disequilibrium offset (0.23‰). If the errors on the coefficients A, B are also taken into account the uncertainty in the SST

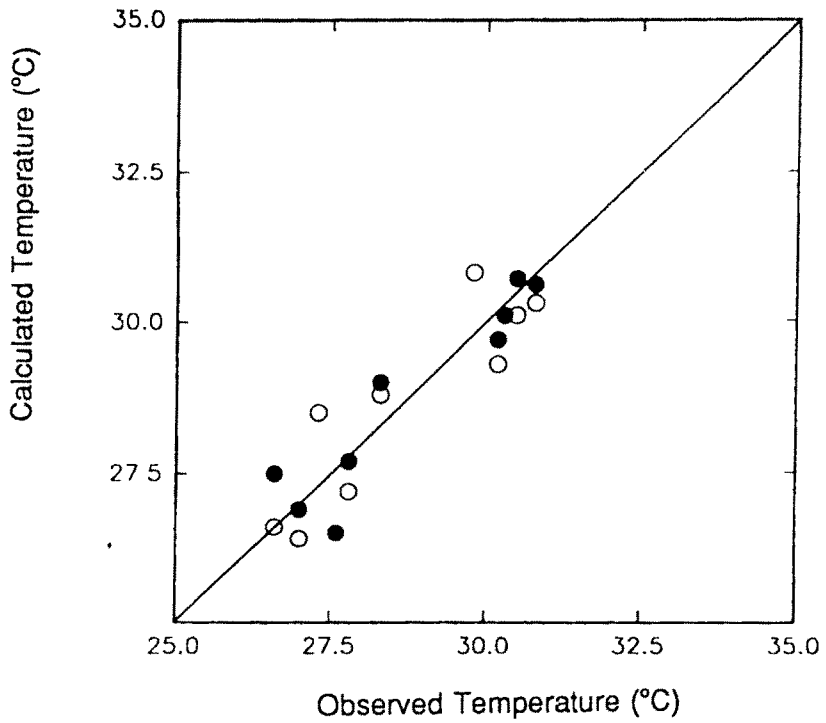

Fig 3.5 Plot of observed vs. calculated SST using coral thermometry. The data appear clustered as they represent the maxima and minima of SST. Filled circle: KV-1, open circle: Am coral. 45° line is drawn for comparison (it is not the best fit line). The observed temperatures are from a location near to the coral site.

estimate becomes 1.9°C. This is the maximum uncertainty in the estimation of SST taking into consideration the errors in δ_w, disequlibrium offset, and in A and B.

Fig 3.5 shows the relationship between observed temperature and the calculated temperature using KV-1 and Am respectively. Please note that even though we have used the Amini coral $\delta^{18}O$ data for calculating the disequilibrium offset, we include these data for comparison because the seasonal variations of the Amini coral $\delta^{18}O$ data have not been used to find the temperature Eqn (3.3). The points scatter closely around the 45° line where the observed temperatures equal calculated temperatures. The mean error in the estimated temperatures is 1.2°C. This estimate is better than that anticipated based on the propagation of errors discussed above.

Now we test this temperature equation by applying it to another *P. compressa* KV-2 from Kavaratti, which had a 25 year long $\delta^{18}O$ record. Its average growth rate based on X-radiography is 15±3.4 mm/yr. We have sampled the bands for isotopic studies to get a resolution of 3 to 6 weeks. (but each sample was ~1mm thick and corresponds to ~1 month growth). Its oxygen isotopic time series is shown in Fig 3.6a and listed in Table III.5 (Appendix-A). Most of the $\delta^{18}O$ values lie between −5.5 to −4.8‰, similar to that observed in KV-1 and Am coral. We use the Eqn (3.4) derived earlier in this section based on the coral data for estimating the yearly maxima and minima in SST. For the $\delta^{18}O$ of water (wrt PDB) for May and Aug we have used values of 0.28 and 0.415 respectively (Fig 3.4b).

Also shown in Table III.4 and Fig 3.7 are observed SST data based on ship record (COADS). Some of the data (during the period 1979-1990) are from Paul *et al.* (1992). As each sample used for $\delta^{18}O$ analysis grew for period of 1 month, the monthly mean values of SST for May ($\delta^{18}O$ minima) and August ($\delta^{18}O$ maxima) are shown in Table III.4, for the sake of comparison. The observed and estimated SST values (from coral $\delta^{18}O$, using Eqn 3.4) are in good agreement within the quoted uncertainty. The difference between the observed and the calculated temperatures has mean values of 0.0±0.9 °C for May and 0.2±0.5 °C for August. The ranges are from −1.7 to 1.7 °C for May and -0.4 to 1.7 °C for August. These are less than the maximum estimated uncertainties of 1.9 °C. Therefore we conclude that our palaeotemperature Eqn 3.4 is quite valid for *P. compressa* in this region. The discrepancy between the observed and calculated temperatures arises

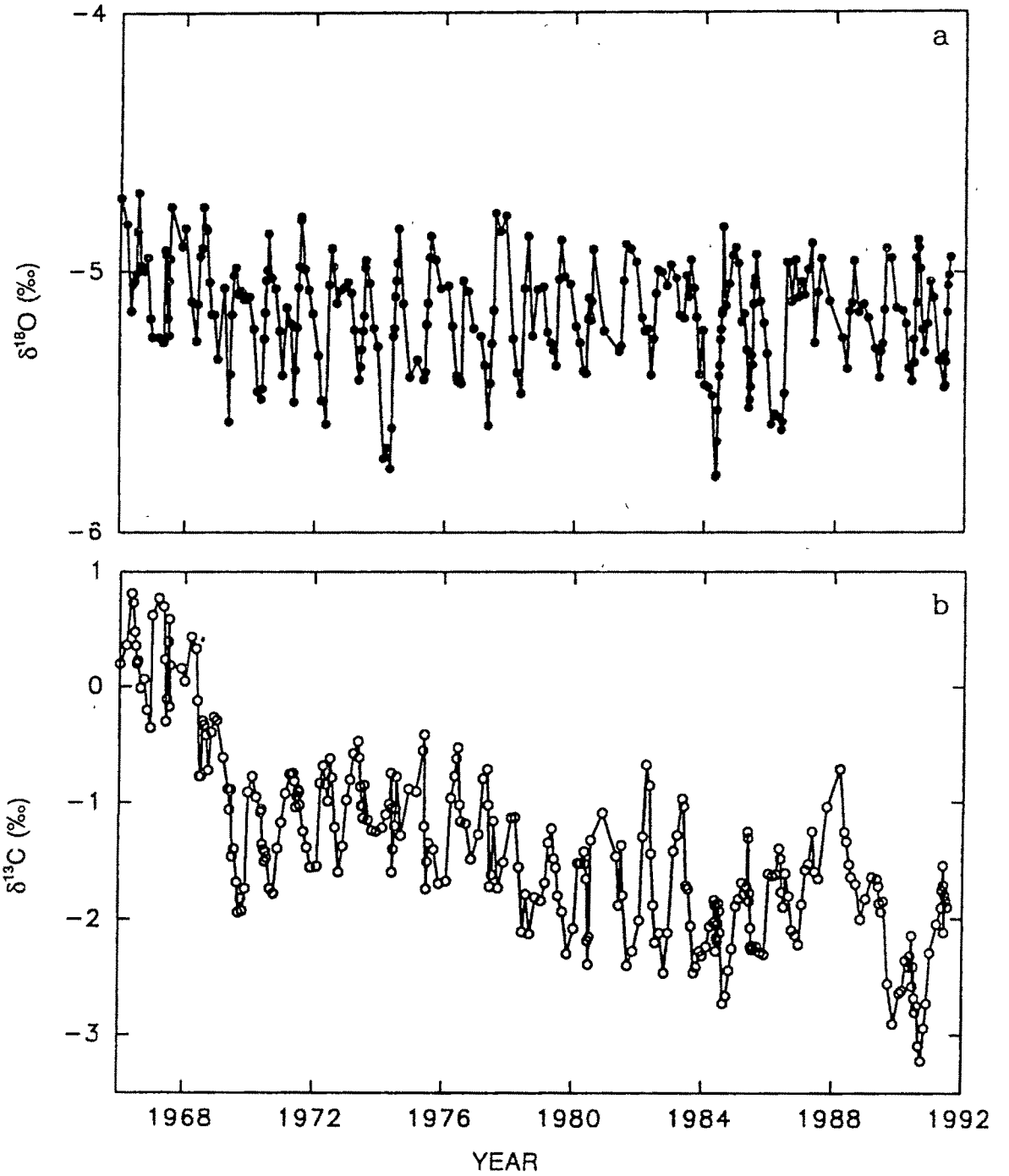

Fig 3.6 $\delta^{18}O$(a) and $\delta^{13}C$ (b) variations in *P. compressa* coral (KV-2) from the Kavaratti lagoon. The $\delta^{13}C$ shows a decreasing trend with age of this coral.

because we have not considered the year to year variations in the $\delta^{18}O$ of water (δ_w). The range of −1.7 to +1.7 °C in the discrepancy, can be caused by interannual variation in δ_w.

Table III.4 Comparison between observed and derived SST

Month & Year	$\delta^{18}O$ (‰)	Derived Temp.T_d (°C)	Obs. Temp.T_o (°C)	T_d-T_o (°C)
May '74	-5.76	31.3	29.8	1.5
Aug '74	-4.84	27.6	27.0	0.6
May '75	-5.41	29.6	29.0	0.6
Aug '75	-4.86	27.7	26.5	1.2
May '76	-5.43	29.7	29.2	0.5
Aug '76	-5.04	28.5	26.8	1.7
May '77	-5.59	30.5	30.1	0.4
Aug '77	-4.78	27.3	27.0	0.0
May '78	-5.46	29.9	30.0	-0.1
Aug '78	-4.86	27.7	27.6	0.1
May '79	-5.30	29.1	29.4	-0.3
Aug '79	-4.88	27.8	27.3	0.5
May '80	-5.39	29.5	30.7	-1.2
Aug '80	-4.91	27.9	28.3	-0.4
May '81	-5.30	29.1	29.9	-0.8
Aug '81	-4.89	27.8	27.5	0.3
May '82	-5.40	29.5	30.2	-0.7
Aug '82	-4.99	28.3	28.3	0.0
May '83	-5.18	28.6	30.1	-0.5
Aug '83	-4.95	28.1	28.5	-0.4

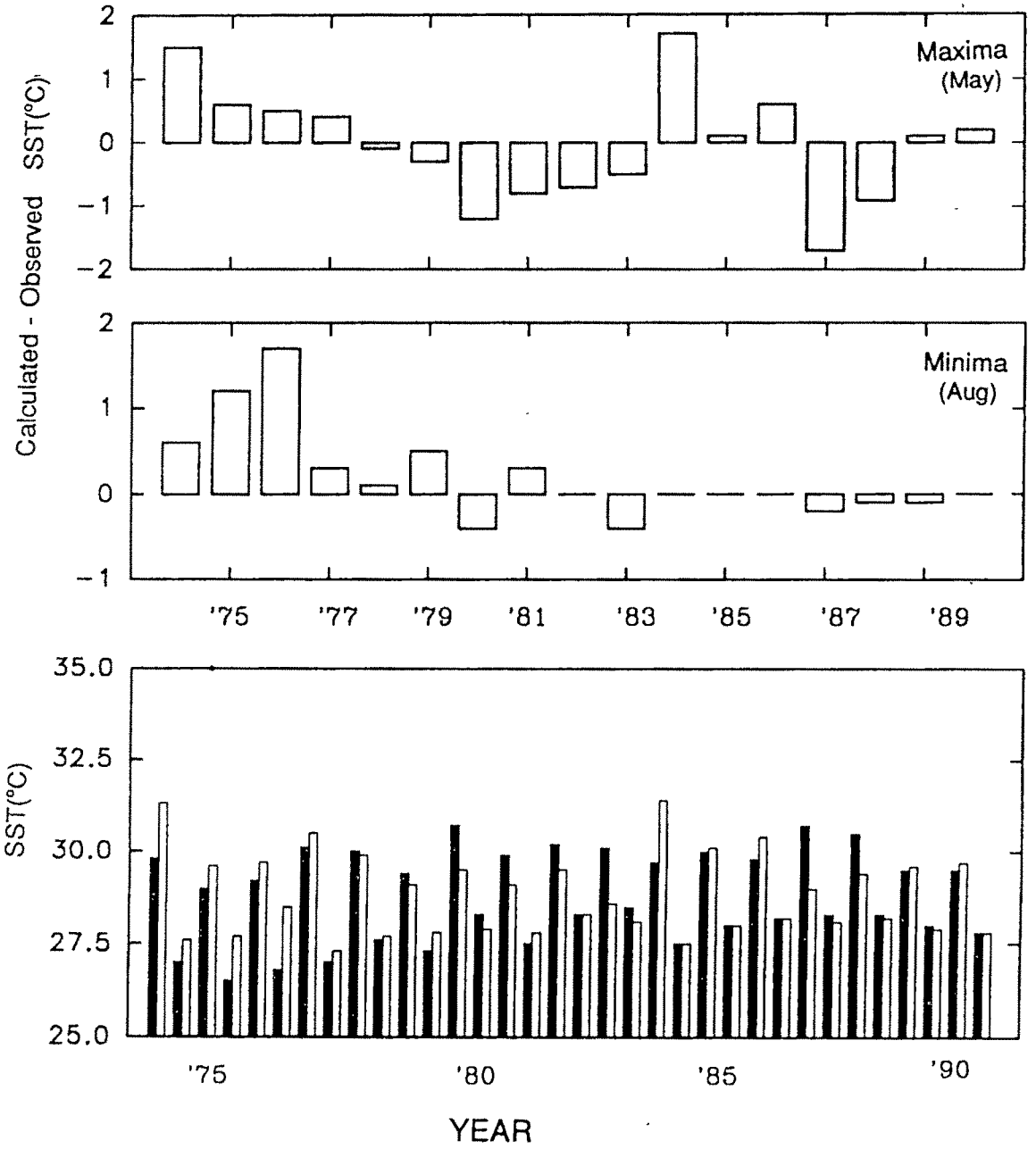

Fig 3.7 Plot showing the observed (filled bar) and calculated SST (open bar) based on coral $\delta^{18}O$ (KV-2). For each year both the minima and the maxima SSTs are shown.

Top panel diagrams show the deviations of the calculated SSTs from the observed SSTs. Deviations for the May has a mean of 0.0±0.9 and for Aug it has a mean of 0.2±0.5 °C.

May '84	-5.79	31.4	29.7	1.7
Aug '84	-4.83	27.5	27.5	0.0
May '85	-5.52	30.1	30.0	0.1
Aug '85	-4.93	28.0	28.0	0.0
May '86	-5.58	30.4	29.8	0.6
Aug '86	-4.96	28.2	28.2	0.0
May '87	-5.27	29.0	30.7	-1.7
Aug '87	-4.95	28.1	28.3	-0.2
May '88	-5.37	29.4	30.5	-0.9
Aug '88	-4.96	28.2	28.3	-0.1
May '89	-5.40	29.6	29.5	0.1
Aug '89	-4.91	27.9	28.0	-0.1
May '90	-5.42	29.7	29.5	0.2
Aug '90	-4.88	27.8	27.8	0.0

Summing up, it can be said that the coral $\delta^{18}O$ thermometry provides a fairly reliable estimation of SST in the LDP region. The uncertainty in the SST estimation is slightly better than the reported uncertainty (±2.8°C) for coral $\delta^{18}O$ as palaeothermometer (Aharon 1991). The present uncertainty of ±1.9°C can be reduced further if we have monthly $\delta^{18}O$ measurements of sea water.

Fig 3.8 shows $\delta^{18}O$ time series of the two corals, KV-1 and KV-2 which grew in nearby regions and which are also of the same species. The data clearly show that there is a close resemblance in their oxygen isotope time series, with almost equal amplitudes for the seasonal variations, ~ 0.8‰. As discussed earlier this seasonal amplitude by and large results from SST changes caused by upwelling during SW monsoon. The magnitude of the $\delta^{18}O$ amplitude for a drought year 1987, was found to be much less, about ~ 0.3‰ in both KV-1 and KV-2. This observation prompted us to look for possible correlation between upwelling and rainfall, both of which are driven by the south-west monsoon. If such a correlation exists then one would expect reduced seasonal amplitude in coral $\delta^{18}O$

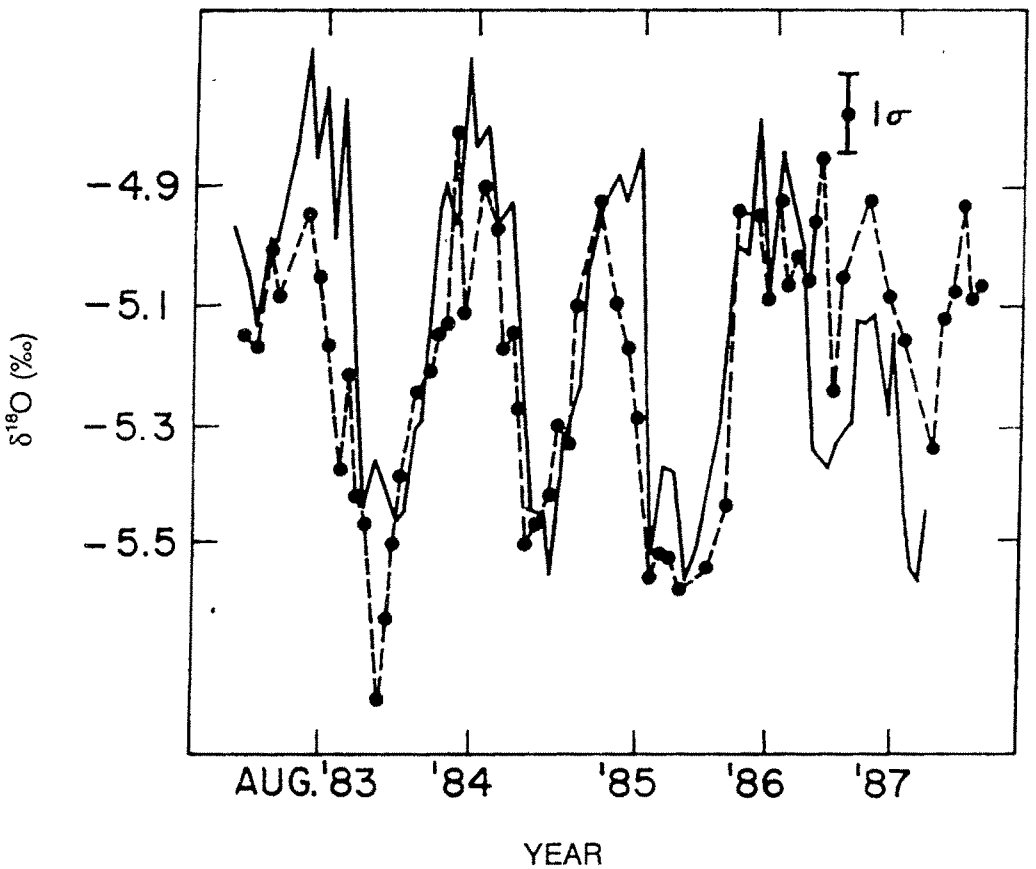

Fig 3.8 Intercomparison of the $\delta^{18}O$ of the two *P. compressa* corals (KV-1, KV-2) from the Kavaratti lagoon, Lakshadweep islands. The two profiles resemble very closely. solid line: KV-1; dashed line: KV-2

in drought years (as seen in 1987) and enhanced amplitude during flood years. To check on this we carefully analyzed the $\delta^{18}O$ amplitude-rainfall trends in KV-2. The results are not conclusive as a consistent trend was not observed. For example the amplitude in the $\delta^{18}O$ for another drought year 1972, did not show a reduction. Similarly the $\delta^{18}O$ amplitudes for flood years also exhibit mixed trends. The years 1971 and 1975 show comparatively enhanced amplitude, but 1983, a heavy rainfall year shows a reduced amplitude. Also, a normal rainfall year, 1984 shows a large amplitude. While the reduction in SST in the LDP region during May-Aug is definitely due to upwelling induced by monsoon winds, the monsoon rainfall on the land is a function of several parameters like moisture content of the air masses entering the land, the distribution of rain over land and sea, orographic features, air temperatures etc. Therefore the upwelling induced SST reduction in the LDP does not appear to be correlated directly with the monsoon rainfall.

In summary, the oxygen isotopic records in *Porites* corals of Lakshadweep region provide a useful tool for monitoring the sea surface temperatures in the past with a reasonable accuracy.

(ii) *Carbon isotopes*

As mentioned earlier the $\delta^{13}C$ of corals is influenced by the isotopic composition of sea-water ΣCO_2, coral growth rate and geometry and biological activities like metabolism and endosymbiotic photosynthesis (Nozaki *et al.* 1978, Fairbanks & Dodge 1979, Aharon 1985, McConnaughey 1989)

The $\delta^{13}C$ time series of corals KV-1 and KV-2 are given in Figs 3.3a and 3.6b respectively and presented in Tables III.3 and III.5 of Appendix A. They show annual periodicities with a seasonal amplitude of ~1‰. We first discuss the seasonal $\delta^{13}C$ variations and the timing of density band formation. This is followed by a discussion on the long term trend in $\delta^{13}C$ in KV-2.

Coral growth is controlled by various parameters. The favourable factors are higher light intensity resulting in enhancement of photosynthesis; corals are carnivores and live on zooplankton, so availability of zooplankton is another favourable factor for coral

growth. On the other hand the parameters inhibiting the growth include water current, turbidity, sedimentation, rainfall and predators. Suresh & Mathew (1993) made *in-situ* measurements on skeletal extension of a reef building coral *Acropora formosa* which grew in the Kavaratti atoll. They measured variations in temperature, pH, salinity, phosphate, nitrate, nitrite, calcium, water current, suspended matter, rate of sedimentation, rainfall and zooplankton activity for the period of 1988-1989 and correlated the coral extension rate with these environmental parameters. They observed that the extension rate of *A. formosa* is directly related to zooplankton and nitrite availability, though the correlation between the growth rate and nitrite is not clear. In the Lakshadweep region zooplankton are more abundant during Dec-Jan and are least abundant during Aug-Oct (*op cit.*). During the monsoon (JJAS) due to stronger water current and enhanced sediment suspension, the growth rate is adversely affected. Also due to the increased amount of cloud cover photosynthesis decreases causing a decrease in photoinduced calcification and hence coral growth. They give supportive evidence to show that the variation in temperature, pH, salinity, phosphate, nitrate and calcium have relatively minor control on the coral growth. Summarizing, the growth rate is slower during the summer monsoon (JJASO) and higher during the rest of the year.

Figs 3.3a and 3.6b show the $\delta^{13}C$ variations of KV-1 and KV-2 respectively. The $\delta^{13}C$ in KV-1 starts decreasing from the beginning of summer *i.e.* in Apr, from -0.07‰ it reduces to -1.25‰. The trend reverses in the month of Dec when its starts rising and reaches a maximum during Jan-Feb. This pattern is also seen in case of the KV-2 coral also, though the absolute $\delta^{13}C$ values of the two corals are different. The ~1‰ dip in the $\delta^{13}C$ in the summer monsoon period can be explained as follows:

The $\delta^{13}C$ of the coral is determined by the $\delta^{13}C$ of the ΣCO_2 of sea-water in the vicinity of coral. This in turn is controlled by (a) zooxanthallar photosynthesis which uses more ^{12}C than ^{13}C and hence enriches the ΣCO_2 of sea-water in ^{13}C; (b) respiration of both the coral and the zooxanthellae, which reduces the $\delta^{13}C$ of ΣCO_2 of sea-water, (c) upwelling of deeper waters due to monsoon, which deplete the ΣCO_2 in ^{13}C by mixing deeper waters depleted in ^{13}C, and (d) oceanic uptake of fossil fuel CO_2 which also depletes the surface water in $\delta^{13}C$. During SW monsoon the cloudiness increases from 60% during May to more than 80% during Jun-Jul (Hastenrath & Lamb 1979). Due to

monsoon activity currents become stronger causing more sediment suspension. In Jul-Aug suspended matter and sedimentation rate in the Kavaratti atoll are increased by about a factor of 3 to 5 (Suresh & Mathew 1993). These effects cause a substantial reduction in the light intensity and therefore the photosynthesis activity of the zooxanthellae decreases to a great extent. As the photosynthesis slows down, photoinduced calcification is also retarded resulting in the formation of the high density band. Probably during this period the respiration dominates over the photosynthesis fixation of carbon. While photosynthesis is carried out only by the zooxanthellae, the respiration is from both the coral polyp and the zooxanthellae. Under these conditions, the $\delta^{13}C$ of coralline $CaCO_3$ is expected to decrease.

By the end of May the monsoon induced upwelling increases and a deeper water component depleted in ^{13}C, is brought along with nutrients like phosphates and nitrates resulting in higher biological productivity in several regions of the Arabian Sea (Sathyendranath *et al.* 1991; Brock & McClain 1992). This causes further reduction in $\delta^{13}C$. Consequently the $\delta^{13}C$ reaches a minimum during Oct or early Nov. This is the time when high density bands cease to form. Again after the monsoon season the light level increases. Turbidity, currents and suspended matter are also reduced causing enhancement in the photosynthetic activity which enriches the coral $CaCO_3$ in ^{13}C. During Dec-Jan zooplankton activity reaches its maximum (Suresh & Mathew 1993). These favourable parameters like increased rate of photosynthesis and higher abundance of zooplankton favour the coral growth which result in low density band formation. During rest of the year the mean cloud content is about 30% and hence the $\delta^{13}C$ values increase by 0.4‰, due to increased zooxanthallar activity.

Therefore the high (HD) density part of the band formed during the monsoon period shows a depletion in $\delta^{13}C$ compared to that of the low density (LD) part. The average $\delta^{13}C$ values for the HD and LD bands are shown in Table III.6. The high density bands, in general show systematic depletion in $\delta^{13}C$ (except in three cases). While comparing these values we use uncertainties corresponding to the standard deviation of the mean, which is 0.02 to 0.07‰ depending on the number of sample per band.

Table III.6 The average carbon isotopic composition of high and low density bands in coral KV-2

Year	Band type	Average $\delta^{13}C$(‰)	Year	Band type	Average $\delta^{13}C$(‰)
1971	HD	-1.11	1980	HD	-1.79
	LD	-1.10		LD	-1.67
1972	HD	-2.42	1981	HD	-1.86
	LD	-1.01		LD	-0.99
1973	HD	-1.14	1982	HD	-1.92
	LD	-0.88		LD	-1.00
1974	HD	-1.19	1983	HD	-2.14
	LD	-0.78		LD	-2.04
1975	HD	-1.27	1984	HD	-2.21
	LD	-1.11		LD	-1.66
1976	HD	-1.10	1985	HD	-2.06
	LD	-0.76		LD	-1.63
1977	HD	-1.45	1986	HD	-1.98
	LD	-1.26		LD	-1.56
1978	HD	-1.88	1987	HD	-1.39
	LD	-1.63		LD	-1.79
1979	HD	-1.90	1988	HD	-2.37
	LD	-1.49		LD	-2.40

Summarizing, the high density band formation takes place during the summer monsoon period viz, Jun-Oct. Due to monsoon activities the growth rate is retarded and the carbon isotopic composition is also depleted. On the other hand the low density bands formed during Nov to May shows a higher growth rate and are enriched in ^{13}C relative to high

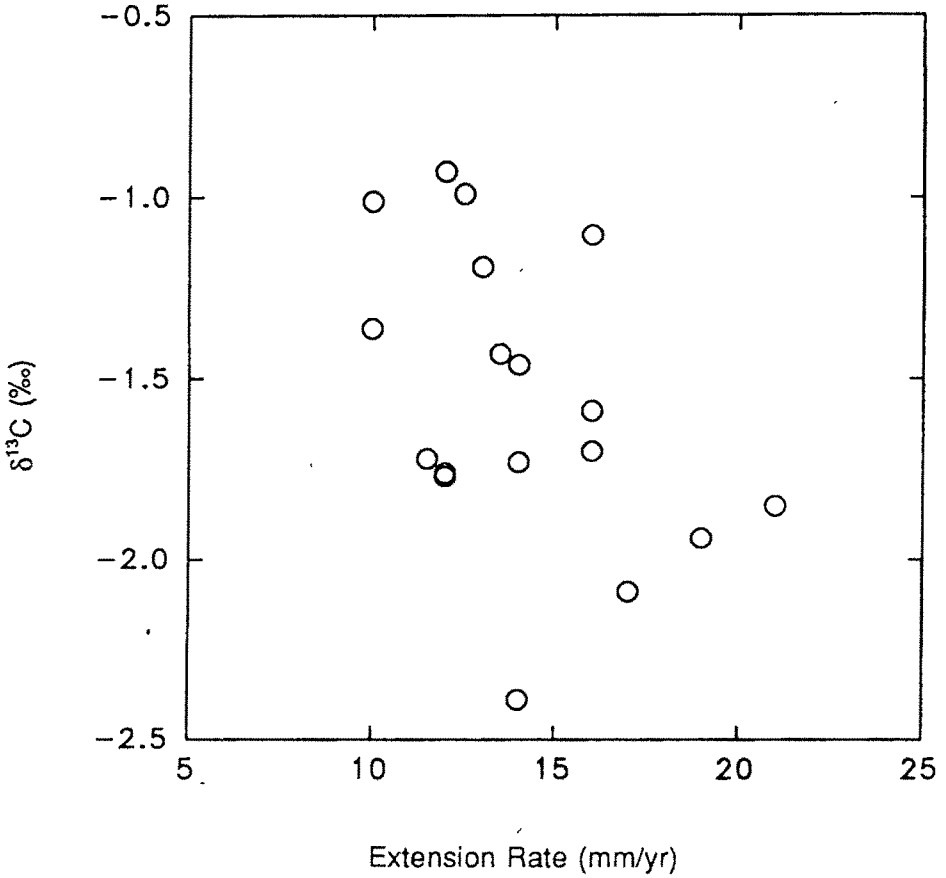

Fig 3.9 Relationship between $\delta^{13}C$ and the extension rate in the coral *P.compressa* (KV-2)

density band. The seasonal variation in $\delta^{13}C$ is caused by the variation in photosynthetic activity of the zooxanthellae, while the variation in growth rate is controlled by environmental parameters as well as zooxanthallar photosynthesis.

On a longer time scale, the $\delta^{13}C$ in KV-2 shows a decreasing trend with time. (KV-1 is only 5 years old and does not show any distinct trend). During the initial stage of its growth KV-2 has a mean $\delta^{13}C$ value of 0.5‰, which decreases to a present day value of ~-2.5‰ (Fig 3.6). It is interesting to note that while $\delta^{18}O$ does not show any trend, $\delta^{13}C$ shows a mean trend of -0.12‰ per year. This is similar to the observations of Aharon (1991) who did not find any trend in $\delta^{18}O$ but a trend of -0.1‰ per year in $\delta^{13}C$ for the Palm Island *Porites*. This large negative shift in $\delta^{13}C$ appears to be affected by the growth rate related fractionation. $\delta^{13}C$ in general shows a negative correlation with the extension rate (Fig 3.9) which conforms to this hypothesis. This growth rate related fractionation is dominant only in interannual time scale; in seasonal time scale the fractionation (of ^{13}C) due to changes in photosynthetic activities dominates over the growth rate dependent fractionation. For this reason despite lower growth rate during monsoon time $\delta^{13}C$ shows a decrement. Growth rate related fractionation was also proposed by McConnaughey (1989) who observed that the faster growing portions of the skeleton suffered more fractionation. However the exact mechanism of this growth rate related fractionation is yet to be fully understood.

Comparison of the mean $\delta^{13}C$ values of KV-1 and KV-2 (both from the Kavaratti lagoon) during 1983-1988, shows distinct differences. The mean $\delta^{13}C$ of KV-1 is -0.75‰ whereas that of KV-2 is -1.8‰. Thus KV-2 is depleted by ~1‰ compared to KV-1. This could be a depth dependent fractionation. KV-1 grew at a depth of ~1m, whereas KV-2 was from a depth of 7 to 10m. According to Fairbanks and Dodge (1979) corals growing at greater depths get less sunlight and hence their photosynthesis rate is also reduced; consequently they are depleted in $\delta^{13}C$ relative to corals growing near the surface. However, this hypothesis is not consistent with our earlier discussion, where higher growth rate is associated with more depleted $\delta^{13}C$. KV-1 has an average growth rate 23.3mm/yr compared to KV-2 which grew slightly slower, 15 mm/yr. This makes it difficult to draw any definitive conclusion about the cause of the difference in the $\delta^{13}C$ values of KV-1 and KV-2 and also about the long term trend (in case of KV-2) resulting from growth rate

dependent fractionation discussed earlier.

Inspite of these difficulties in explaining the carbon isotopic variations we see that the $\delta^{13}C$ of the *Porites compressa* from Lakshadweep region shows a general behaviour, the seasonal cyclicity due to variations in the photosynthesis modulated by monsoonal activities. This seasonal dip in the $\delta^{13}C$ during monsoon and the enhancement of $\delta^{18}O$ during the same season due to cooling, induced by upwelling may provide clues to the past upwelling changes, once quantified.

III.2.b Gulf of Kutch coral

The Gulf of Kutch coral (GK) belongs to the genus *Favia*. Its life span based on X-radiography was 41 years with an average growth rate 4.3±1.3 mm/yr.

The carbon and oxygen isotopic data of samples from annual bands of the Gulf of Kutch coral is presented in Fig 3.10 [data in Appendix-A, Table-III.7]. It is known that the $\delta^{18}O$ of coral carbonate is determined by (a) SST and (b) $\delta^{18}O$ of the water in which it grows (often when $\delta^{18}O$ data for sea water is not available, salinity is used as an index of $\delta^{18}O$ as these two in general, are correlated (Craig & Gordon 1965); however this relationship differs from region to region and has to be established for each specific area). To determine the utility of the coral $\delta^{18}O$ data for retrieving climatic parameters we need to know how the $\delta^{18}O$ of coral responds to the local sea surface temperature and $\delta^{18}O$ variations. To quantify these effects for the GK coral we use COADS SST data (Sadler *et al.* 1987) at 22.6°N, 69.5°E, closest available to the Gulf of Kutch. The curve (Fig 3.11) shows maximum SST (29°C) around June and minimum (23°C) around Jan-Feb. During Aug-Sep there is a small trough, (~2°C) which could be due to reduction in air temperature resulting from monsoon activity and the lateral transport of upwelled cooler waters from the open ocean into the Gulf. The $\delta^{18}O$ of sea water (relative to PDB) from the coral location was measured periodically (Nov, Dec 1992, Jan, Feb, May & Jun 1993). The values range from 0.39‰ (December) to 0.71‰ (May). Based on these SST and $\delta^{18}O$ of water (δ_w) data we calculate the seasonal amplitude in the coral $\delta^{18}O$ to be 1.1±0.2‰, with a maximum in January and a minimum in June. For making this

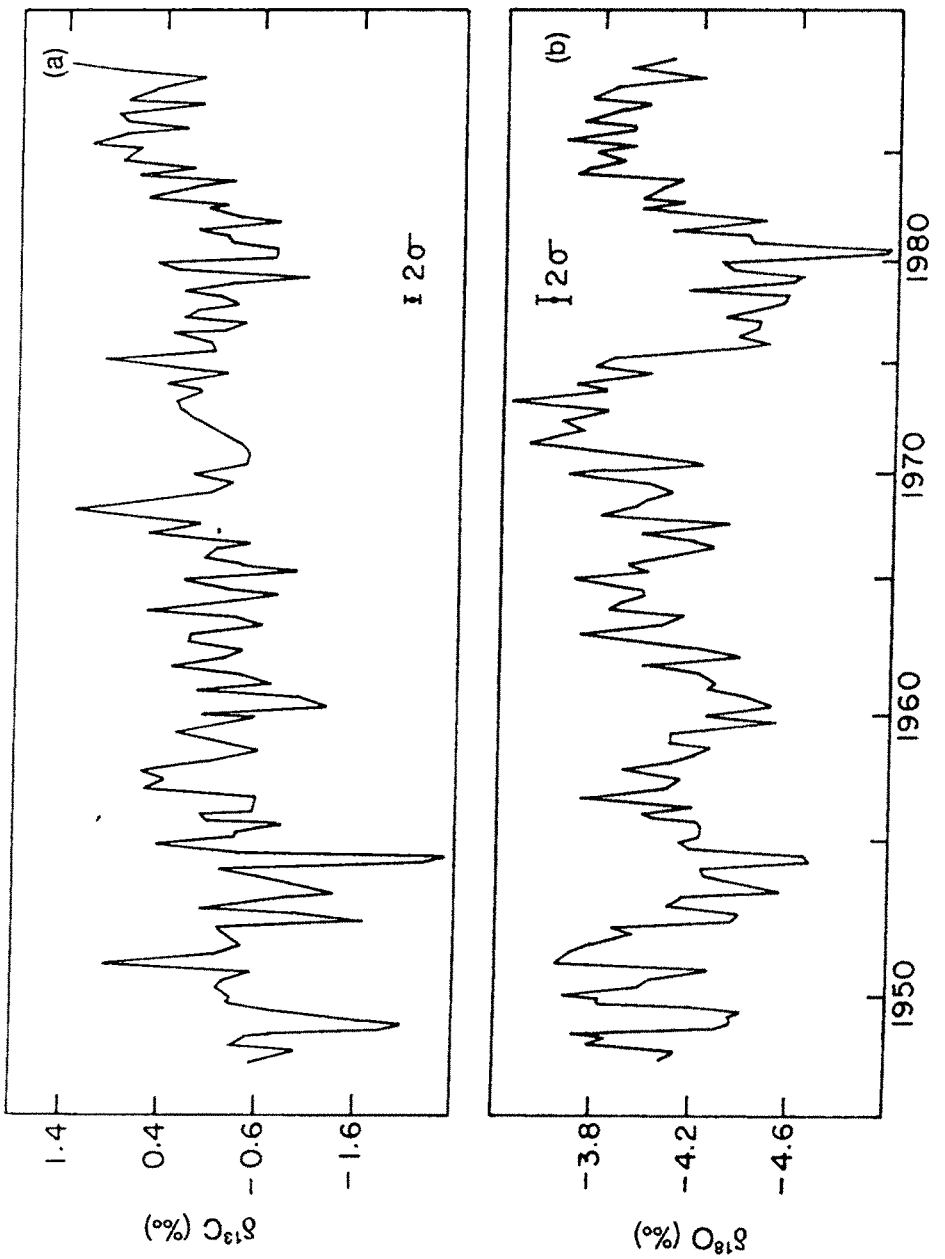

Fig 3.10 $\delta^{13}C$ (a) and $\delta^{18}O$ (b) records of the coral *Favia speciosa* (GK) from the Gulf of Kutch (22.6°N, 70°E)

calculation we have used the relation between SST and $\delta^{18}O$ for this coral species (Weber & Woodhead 1972, temperature coefficient –0.239‰ $°C^{-1}$) and adjusting for the sea water $\delta^{18}O$ variation: 6 °C change in SST would correspond to 1.43‰ change in the coral $\delta^{18}O$. The change in $\delta^{18}O_w$ of 0.32‰ would act in the opposite direction and reduces the coral $\delta^{18}O$ amplitude to 1.1‰. The observed mean seasonal $\delta^{18}O$ amplitude is only 0.3±0.2‰ much less than the calculated value. The apparent discrepancy between the observed and calculated $\delta^{18}O$ amplitude could be due to the low resolution sampling resulting from the slow growth rate. This is discussed later based on a model simulation study. The seasonal amplitude is superimposed on an apparent higher order cyclicity of 7-8 years.

It is well established that the coralline $\delta^{18}O$ is controlled to a large degree by SST. If there is any relation between SST and rainfall it is likely that the coralline $\delta^{18}O$ would also mimic such a relation. To asses this we have compared the $\delta^{18}O$ and $\delta^{13}C$ of the Gulf of Kutch coral with the rainfall data.

Fig 3.12 shows the minima (corresponding to June) in $\delta^{18}O$, $\delta^{13}C$ and the total monsoon rainfall (approximately same as the annual rainfall) in Kutch for the period 1949-89 A.D. (India Meteorological Division's Records). Kutch and Saurashtra receive almost the entire amount of annual rainfall during the monsoon period (June to September). It can be seen from Fig 3.12 that there is in general negative correlation between the $\delta^{18}O$ minima and rainfall. The relationship between the coral $\delta^{18}O$ (minima) and rainfall is given by:

$$\delta^{18}O = -3.9 - 6.5 \times 10^{-4} R \qquad (3.6)$$

where R represents rainfall in mm. The correlation coefficient (r) is -0.56 (n=41) significant at 0.01 level (P). As the numerical ranges of variation in $\delta^{18}O$ (0.3‰) and rainfall (1170 mm) are widely different, we can normalize each of these time series by subtracting the respective means and dividing by the respective standard deviations; this makes both the time series to have identical numerical ranges in variation. (This transform, known as Z transform in statistical literature, makes the mean and standard deviation of the time series to be zero and unity, respectively). Denoting the time series now by $\delta^{18}O'$ and R', we get a relationship (with the same correlation coefficient as earlier):

$$\delta^{18}O' = -0.51 R' \qquad (3.7)$$

In order to produce a change of 0.1‰ (detection limit) in the coral $\delta^{18}O$ rainfall has to

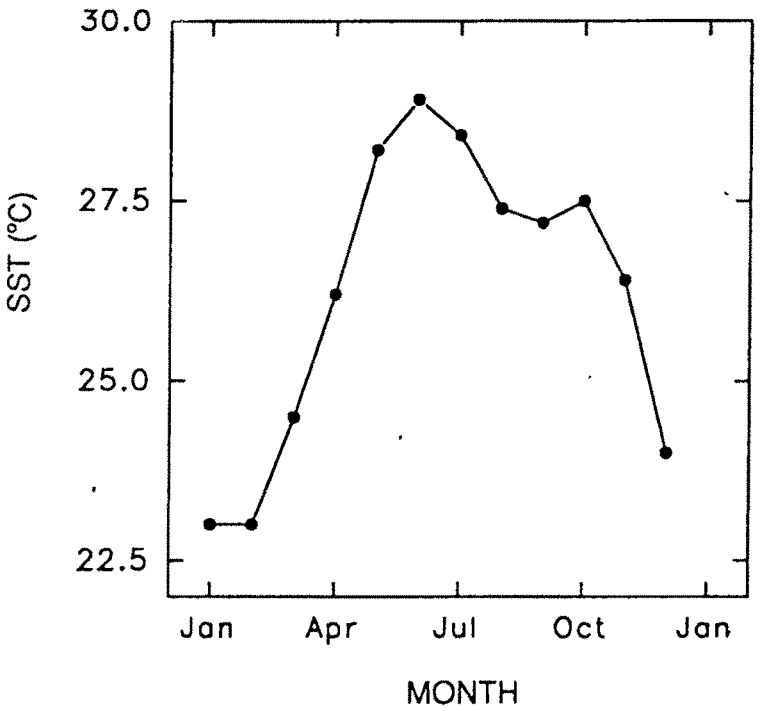

Fig 3.11 Monthly SST variations in the Gulf of Kutch (22.6°N, 69.5°E), near to the coral site. Data from Sadler *et al.* (1987).

change by ~150 mm. The magnitude of year to year variation in rainfall is ~340 mm (one standard deviation, which represents the interannual variability). This will cause a mean interannual change in the coral $\delta^{18}O$ of a magnitude 0.22‰. Moreover, the difference in rainfall between two consecutive years can be as large as -700 to +950 mm, as seen from the rainfall record for the period 1949-89 A.D.; therefore the corresponding changes in the coral $\delta^{18}O$ can be as large as +0.46 to –0.63‰. We have not been able to observe such large changes in the $\delta^{18}O$ record. One possible explanation for this may be coarse resolution of sampling which averages out large changes. This coral has an average growth rate of ~ 4 mm/yr and a sample of ~1mm thickness corresponds to about 3 month's growth.

The long term changes (*e.g.* 7 to 8 year cyclicity) in the coral $\delta^{18}O$, (Fig 3.10a) may be caused by the long term changes in rainfall. For example the consistently higher than normal rainfall during the late 70's is reflected as a dip in the coral $\delta^{18}O$ (Fig 3.12). In order to have a definitive explanation of the periodicity of 7 to 8 years, we need a time series measurement of the $\delta^{18}O$ of sea water before and after the monsoon, which is lacking for this region.

The dotted lines in Fig 3.12 a,b and c are fourth order regression lines through the data representing the trends. We used the trend lines to generate points of $\delta^{18}O$ and rainfall and found them to be correlated better: $r = -0.8$ ($n=41$). This shows that while the long term changes in the coral $\delta^{18}O$ are related to rainfall, seasonal variations tend to introduce noise in the signal. In addition, the mean annual $\delta^{18}O$ of the coral is also significantly correlated with monsoon rainfall over Kutch and Saurashtra ($r = -0.48$, $P < 0.01$) as well as the all India mean monsoon rainfall ($r = -0.23$, $P < 0.1$). This observation is consistent with the theory of Shukla (1975) and observations of Shukla & Mishra (1977) that the increase in SST (reduced coral $\delta^{18}O$) in the Arabian Sea enhances the evaporation rate and hence the precipitation over India, especially in Gujarat. From the $\delta^{18}O$ record we see that the mean difference in the $\delta^{18}O$ in decadal time scale (~0.48‰) would correspond to a change of 2.4°C in SST. From this it appears that the GKh responds to long term changes in SST probably because of its shallow shelf characteristics. On the other hand the LDP region which is exchanging water with the open Arabian Sea freely, does not show such large long term trends in SST and therefore

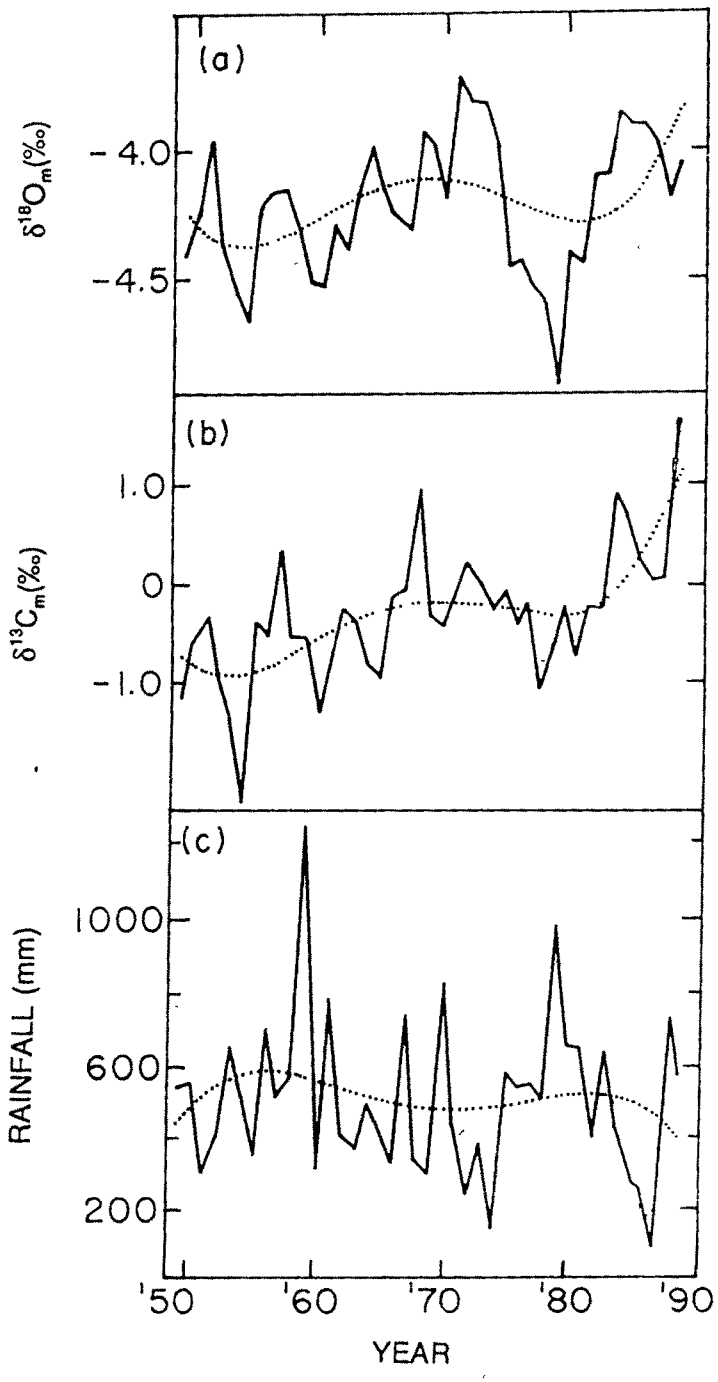

Fig 3.12 $\delta^{18}O$ minima (a), $\delta^{13}C$ minima (b) of the coral *F. speciosa* from the Gulf of Kutch (22.6°N, 70°E). Lower panel (c) shows the interannual variability of monsoon rainfall in the Kutch and Saurashtra region. The dotted lines are fourth order polynomials fitted to the data and indicates the long term trends.

in $\delta^{18}O$. Hence in the case of LDP coral the $\delta^{18}O$ is not correlated with monsoon rainfall.

The mean $\delta^{13}C$ of the GK coral is ~ –0.1‰. Both KV-1 and KV-2 are depleted by about 0.6 and 1.7‰ respectively compared to GK coral. Comparison of the KV-2 data with GK coral is more meaningful as the GK and KV-2 corals had approximately similar life span. The causes for the difference in the $\delta^{13}C$ between these two corals are (i) the species dependent fractionation, (ii) the northern Arabian sea, especially the coastal regions are biologically more productive compared to the central and south-eastern Arabian Sea (Qasim 1982) and the $\delta^{13}C$ of ΣCO_2 here are expected to be higher than that of the LDP region, and (iii) growth dependent fractionation. The mean growth rate of the GK coral is 4.3 mm/yr whereas that of the KV-2 is 15mm/yr. Since slower growth rate leads to isotopic values which are closer to equilibrium precipitation, the GK coral shows a higher $\delta^{13}C$ compared to the KV-2 coral.

The $\delta^{13}C$ values of the GK coral show a long term increase of about 2‰ during the 40 years of its growth, from ~ -1‰ during its early stage of growth to the present day value of ~1‰. The mechanisms contributing to this long term trends is not well understood, growth-rate related ^{13}C fractionation may be one of the contributors to this trend. In the earlier stage of growth the mean growth rate was higher (~ 6 mm/yr) whereas in the later stages the mean growth rate is between 3-4 mm/yr (Fig 3.2). This would contribute to enrichment of $\delta^{13}C$ during the later stages.

The $\delta^{13}C$ of GK coral shows a seasonal cycle, with a range of ~1‰. The minimum in $\delta^{13}C$ occurs during Jun-Jul, approximately at the same time when the minimum in $\delta^{18}O$ occurs. In fact $\delta^{13}C$ and $\delta^{18}O$ are significantly positively correlated (r=0.56). The reason for minimum in $\delta^{13}C$ during Jun-Jul is probably due to the reduced rate of photosynthesis during this time of the year compared to the pre SW monsoon (Feb-May) and post SW monsoon (Oct-Jan) seasons.

Qasim (1982) has observed that in general the phytoplankton productivity is high in the coastal regions of the northern Arabian Sea. The average surface productivity for this region is 18.86, 7, and 25.12 gC m^{-2} day^{-1} for the premonsoon, monsoon and NE monsoon period respectively (Table 8 of Qasim 1982). The lowest biological productivity during SW monsoon period, probably leads to a depletion in the coral $\delta^{13}C$ during this period. Thus the seasonal changes in $\delta^{13}C$ in GK coral hold potential to reconstruct past

changes in surface productivity in this region. Towards this, it is necessary to establish quantitative relation between $\delta^{13}C$ and biological productivity of this region.

III.2.c Effect of sampling on the retrieval of climatic signal

The retrieval of climatic information from the isotopic profiles of coral depends largely on the sampling resolution. Early studies of $\delta^{18}O$ records as an SST index were not much successful as observed by Goreau (1977) and Emiliani *et al.* (1978). This apparent drawback of isotopic study was attributed to the (sampling) resolution problem by Fairbanks & Dodge (1979). They showed that with the analyses of as much as 12 samples per annual band they were able to recover the full seasonal amplitude of SST from the $\delta^{18}O$ measurements. Lesser the number of samples, more are the chances of missing the maxima and minima in the $\delta^{18}O$. Moreover, in the case of very narrow annual bands, it is difficult to get more than a few samples per band for isotopic analyses. Further, a sample taken by filing or drilling has a finite width (say, 1 mm), which, in the case of a narrow annual band can average the SST signal for a period of as much as 6 months. Thus depending on the sample growth rate (*i.e.* the skeletal extension rate) and the sampling interval, the measured seasonal $\delta^{18}O$ amplitude can be greatly reduced compared to its actual value. In order to assess the magnitude of this reduction, we performed a simple computer simulation.

Since the seasonal $\delta^{18}O$ profile very closely resembles sinusoidal variations, we generated 20 cycles of a sine wave of unit amplitude and a (spatial) period of 10 mm. This would correspond to a $\delta^{18}O$ time series of a coral having a 20 year growth with an annual growth increment (g) of 10mm. Implicit in our use of unit amplitude throughout the 20 cycles is that the seasonality in climate forcing did not change during this period (*i.e.* interannual variability is zero). Also, the constant period represents a constant annual growth increment throughout the 20 years of the coral's life span. In the model we sample this time series for different constant sampling intervals Δx (1, 2, 3, 4 and 5 mm) and consider the sample as a point). The maxima and minima in this sampled time series are identified (Fig 3.13). The sum of the magnitudes of the maxima and minima in each

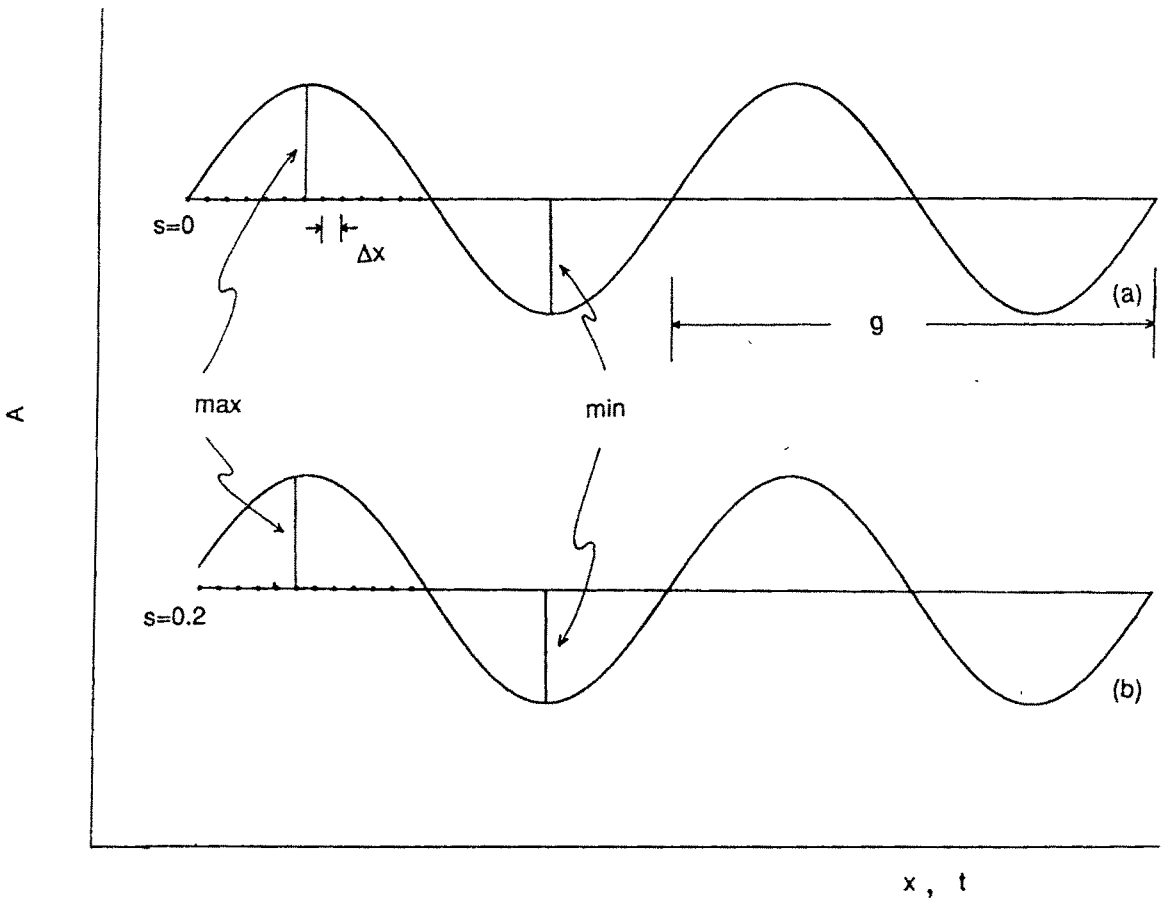

Fig 3.13 Sampling of coral for oxygen isotope study. The seasonal oxygen cycles mimic sine curve. s is the starting (or phase) of the sampling. (a) s=0 *i.e.* phase=0 and (b) s=0.2 or phase=7.2°. Δx is the sampling interval and g stands for annual growth increment.

cycle is divided by 2 to obtain the mean amplitude for each cycle. Then the average of these mean amplitudes over the 20 cycles is calculated and is termed as the 'retrieved amplitude'. We establish a functional relationship between $\Delta x/g$ (reciprocal of the number of samples per band) and A (the ratio of the retrieved amplitude to the actual amplitude). Obviously, A has to be ≤ 1, because the sampling process tends to reduce the signal and at best can reproduce the actual amplitude. The ratio A gives an estimate of the reduction in the amplitude resulting from variation in sampling interval for a constant annual growth increment. In practice when the coral is collected, the last year's annual cycle may not be complete. So the sampling need not commence at the phase=0 of the sine wave. Therefore the exercise was repeated (i) for different starting values of the distance of the first sampling point s, (*i.e.* different phases) and (ii) for different g's (periods of 5 and 10 mm).

Fig 3.14 shows a plot of A versus $\Delta x/g$ when g=5mm. Circles denote the values of A for the sampling case when s=0, *i.e.* the sampling was started with phase zero and inverted triangles and squares denote cases when sampling was started at phases of 14.4° and 36° respectively. (This was achieved by starting the sampling at distance of 0.2 and 0.5 mm respectively from the origin).

It is obvious that when $\Delta x/g=0$ (*i.e.* infinitely close sampling) we retrieve the full amplitude (*i.e.* A=1) and when $\Delta x/g=0.5$ or 1 (*i.e.* the sampling interval is half or full period) the retrieved amplitude should be zero, if the sampling starts from origin (*i.e.* zero phase). This is seen in Fig 3.14: A=1 at $\Delta x/g=0$ and A=0 at $\Delta x/g=0.5$ and 1(for g=5mm). For the rest of the values of $\Delta x/g$ the values of A lie between 0 and 1. As $\Delta x/g$ increases, there is a general reduction in A. For example, when $\Delta x/g=0.2$, 5% of the amplitude is lost due to sampling and when $\Delta x/g=0.8$, 60% of the amplitude is lost. For the other cases when the sampling was started with non-zero phase, the general trend is the same. However for $\Delta x/g=0.5$, we do get A values above zero. This is because the sample points do not lie on the zeros of the sine curve, but slightly off the zeros providing some "amplitude". Further as the phase increases from 0 to 36°, the scatter in A increases around $\Delta x/g=0.5$ and 1. Higher the starting phase, higher is the retrieved amplitude (in these two points). Similar results are shown in Fig 3.15 for the case g=10 mm. As before here also it is seen that A tends to zero as $\Delta x/g$ equals 0.5 or 1. Fig 3.16 shows a plot of A versus g for different $\Delta x/g$ values. It is seen that for a starting value zero (*i.e.* phase=0) A is only

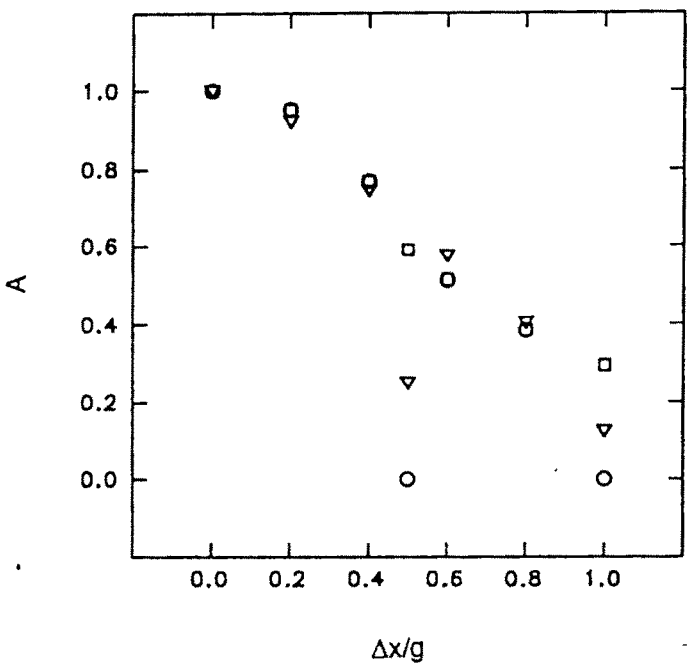

Fig 3.14 Result of the simulation study. Variation in the ratio of the retrieved amplitude to the true seasonal amplitude as a function of Δx/g (the ratio of sampling interval to constant annual increment=5 mm). Different symbols indicate different sample starting(s). Open circle; s=0; inverted triangle: s=0.2; square: s=0.5. For Δx/g=1 (i.e. sampling interval same as annual growth) and s=0, A becomes equal to 0. A increases from zero with increasing s.

a function of $\Delta x/g$ and not g itself. However A shows a small variation with $\Delta x/g$ when sampling is done at non zero phases. If a 10% reduction in amplitude is accepted, then $\Delta x/g$ must be at least about 0.3 *i.e.* approximately a minimum of 4 samples per annual band.

In another simulation, we assumed that while year to year climatic changes are absent, the annual growth increment varies in a random fashion between 2.5 to 5 mm (similar to the growth rate variation in the Kutch coral; growth rate varies due to changes in environmental parameters *e.g.* supply of nutrients). Since the sine function has a constant (spatial) period, a variable growth cannot be represented by a single function. In order to circumvent this problem we generated single cycle of 20 sine functions of unit amplitude but with varying period 2.5 to 5 mm. Then we made the composite function by putting the sine functions in the same time sequence as their growth rates in the case of GK coral. The end points of the cycles match because the value of the sine function in a full cycle is zero at either ends $(0, 2\pi)$. This curve is then sampled to obtain A as before for different Δx (1, 2, 3 and 4 mm) and s (0°, 18°, 45°). In this case $\Delta x/g$ is not a constant as g varies with time. Therefore we plot A as a function of $\Delta x/\bar{g}$, where $\bar{g}$ is the average of all g's (~4 mm). Fig 3.17 shows the composite plot. We see similar trends as in the earlier case of constant growth increment. Also in general the reduction in amplitude is more or less the same as in the previous case. As shown earlier that A is independent of g but only a function of $\Delta x/g$ (for phase=0). In this case for $\Delta x/g$ =0.2 we get A=0.92±0.068 which is the same within the uncertainty to that of A(0.951) for $\Delta x/g$=0.2 when g is constant. However direct comparison is slightly difficult because for the cases $\Delta x/g$ =0.5 and 1 we get significantly higher values of A even for the case when the sampling starts at zero phase. This is understandable because the annual increment is varying and therefore even for the case s=0, some "amplitude" will be retrieved for $\Delta x/g$=0.5 and $\Delta x/g$=1.0.

In addition to the sampling interval, another factor which reduces the retrieved amplitude is the averaging of the signal due to finite sample thickness. We considered the effect of sampling thickness on the amplitude in the following way: we sampled the data generated for the variable growth rate at different intervals, but now by averaging 1 mm around each sample. For this case the reduction in amplitude was found to be 40% for

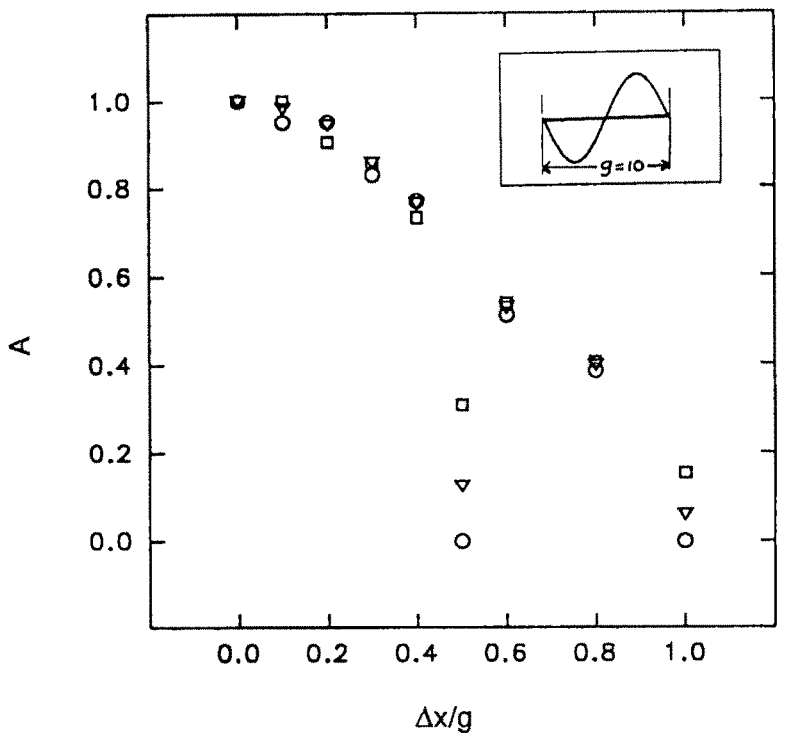

Fig 3.15 Results of the simulation study. Variation in the ratio of the retrieved amplitude to the true seasonal amplitude as a function of Δx/g for the constant annual increment g=10 mm. Symbols indicate different starting of the sampling(s). open circle: s=0; inverted triangle s=0.2; square: s=0.5. As shown in the inset that at Δx=5 and 10, A is zero (for s=0), but with increasing s, A increases at these two points.

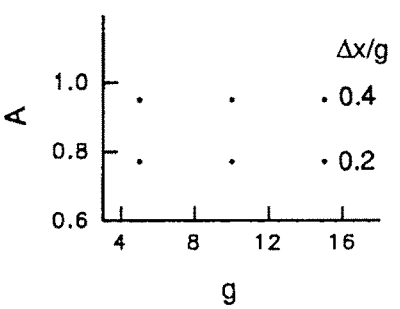

Fig 3.16 Figure shows that the retrieval of amplitude is independent of growth (for zero starting of sampling) but depends on the sampling frequency. Parameters are as described before.

a $\Delta x/\bar{g}$ value of 0.38 very similar to that in the GK coral. Using this we can compute the approximate magnitude of the actual seasonal $\delta^{18}O$ amplitude in the coral studied by us. The observed amplitude(0.3‰) can be considered as 60% of the expected amplitude, therefore the original amplitude can be deduced to be 0.5±0.3‰. This is still about a factor of two less than the calculated amplitude of 1.1±0.2‰ based on SST and the seawater $\delta^{18}O$ variations. Considering that there is an uncertainty of 0.2‰ in the measurements (as in case of the $\delta^{18}O_{water}$) and hence in the estimate, it may be argued that the expected and observed $\delta^{18}O$ amplitudes are comparable within $\pm 2\sigma$ uncertainties. However, they could be genuinely different for reasons other than sampling. These include (i) The model does not consider year to year changes in $\delta^{18}O$ of sea water that may be caused by rainfall (or minor discharges from seasonal rivers), (ii) The calculated coral $\delta^{18}O$ amplitude may be an over estimate as (a) the temperature coefficient for our sample may be different from the value we have used, the value reported by Weber & Woodhead (1972); which is the only available data in the literature for the genus *Favia*. However, there may be variations from species to species and from place to place. For instance McConnaughey (1989) reported temperature coefficients deviated by about 30% *i.e.* 0.205 and 0.15 for *Pavona clavus* samples, one from Champion Island and the other from Punta Pitt, separated by 100 km; (b) We do not have the SST data in the exact location of the coral. Notwithstanding the above possible uncertainties, we get a reasonably good agreement between the calculated and observed $\delta^{18}O$ amplitudes.

Our results show that the coralline $\delta^{18}O$ and monsoon rainfall are significantly correlated, which can be used for qualitative reconstruction of historical rainfall records and also help understand the role of the Arabian SST in determining the interannual variability of monsoon rainfall over western India. Further higher resolution studies on the Gulf of Kutch corals spanning longer time durations will be useful for such a goal. It is necessary that a very close sampling be done for the $\delta^{18}O$ analysis in order to retrieve the full seasonal cycle. The $\delta^{13}C$ variations can be a potential indicator of the past surface ocean productivity in this region. In contrast to *Porites* of Lakshadweep the growth related fractionation is less. We have developed a simple model using which it is possible to estimate the reduction in the retrieval of seasonal amplitudes resulting from the averaging and sampling effects.

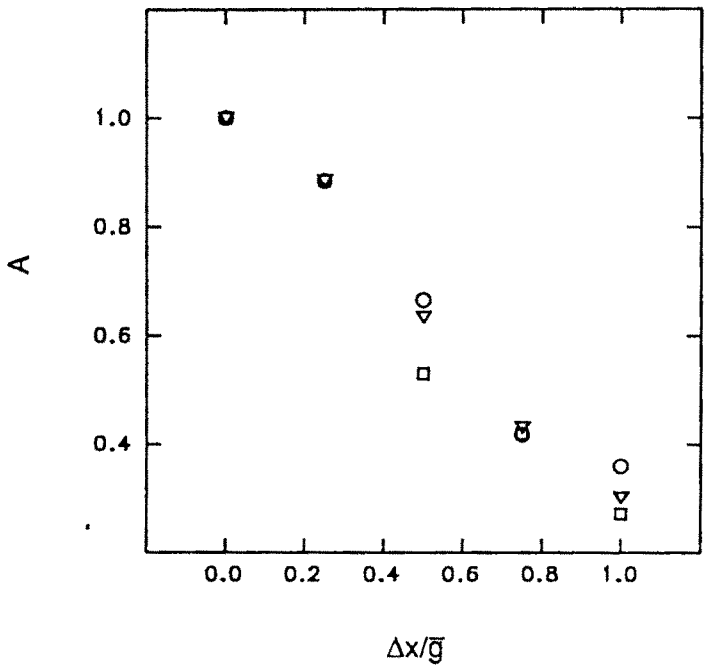

Fig 3.17 Plot of the variation in the ratio of the retrieved amplitude to the true seasonal amplitude as a function of $\Delta x/\bar{g}$ for the variable annual increment (g). Since g is varying, it has been replaced by average g i.e. $\bar{g}$. Unlike the case of constant growth here A does not become zero at $\Delta x=\bar{g}/2$ or at $\bar{g}$ because of variable nature of g. However at these points A shows a wide scatter for different starting values as was observed in case of constant growth.

III.2.d Stanley Reef coral

A coral *Porites lutea* was collected in December 1988 from the Stanley Reef (19°15'S, 148°07'E), belonging to the Great Barrier Reef, Australia. The coral was about 20 years old and had an average bandwidth of 11.7±0.3 mm as determined from the X-radiographic analysis. In order to determine the extent of intraband isotopic and density variability and their effects on respective records we have analyzed the $\delta^{18}O$, $\delta^{13}C$ and density time series in two tracks of this coral.

It is believed that the coralline isotopic records are influenced by the coral geometry and growth rate. In order to minimize the growth related fractionation it is customary to sample along the axis of maximum growth. However due to various constraints sometimes it is difficult to comply with these requirements. In such cases it is important to know the magnitude of intraband isotopic variability and the factors controlling such variations, *i.e.* climate (external forcing) and non-uniform growth in different directions (internal forcing).

Secondly, the reason for the density band formation in corals has not been clearly understood. For example, Highsmith (1979) and Weber *et al.* (1975) concluded that the density banding is mainly controlled by SST. Others (Buddemeier, 1974; Wellington & Glynn, 1983) have attributed the seasonal variation in growth rate to be the cause of the density banding. But then, growth rate itself may be controlled by the SST. It should be possible to decide between these two alternatives by measuring the stable isotope ratios of oxygen ($\delta^{18}O$) and carbon ($\delta^{13}C$) along with the density measurements in the same coral. If the density banding is synchronized with the water temperature, there should be a significant correlation between density and oxygen isotope variations as the latter is related to temperature. On the other hand if the variable growth rate is responsible for the density banding, the density and carbon isotopic variations should be significantly correlated. This is because faster growth rates imply rapid zooxanthallar activity (photosynthesis) which enriches the ^{13}C in the dissolved inorganic carbon in the neighbourhood of the coral, by removing preferentially the more of the lighter isotope of carbon (^{12}C). Thus the $CaCO_3$ secreted by the coral skeleton is enriched in the $^{13}C/^{12}C$

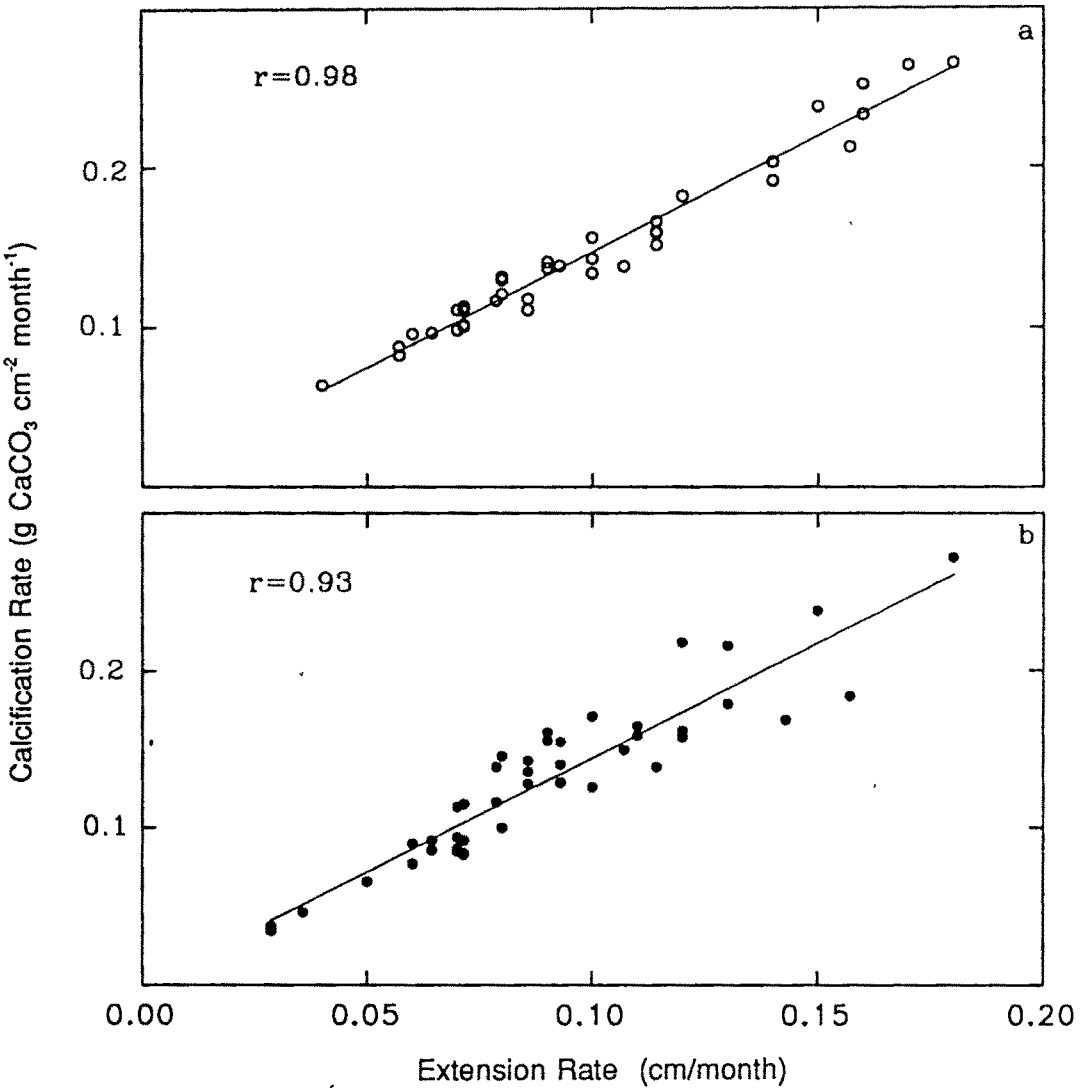

Fig 3.18 Relationship between calcification rate and extension rate of two tracks of coral *P. lutea* collected from the Stanley Reef, east coast of Australia. (a) Track-1, (b) Track-2. The linear trend is clearly evident.

ratio. Again the $\delta^{13}C$ is also controlled by variability in growth rate *i.e.* more the growth rate more will be the $\delta^{13}C$ fractionation. Clearly the rate of photosynthesis and the rate of growth oppose each other in determining the coral $\delta^{13}C$. The ultimate ratio would be determined by the variable contributions of these two parameters. Precise estimation of the fractionation factors between aragonite-water-bicarbonate system for these two cases would enable to determine their relative contribution which is beyond the scope of this work.

The X-radiography and sampling for stable isotopic measurements were followed as described in previous chapter. The density was measured by J M Lough at the Australian Institute of Marine Science following the procedure described by Barnes & Lough (1989). One of the tracks(Tr-1) was ~10° off the central growth axis, and the other (Tr-2) was away from the growth axis by about 20°. For stable isotopic measurements the sampling was performed along the two tracks approximately at high and low density points. Tr-1 and Tr-2 had 3-4 and 2-3 sampling points per annual band respectively.

The use of growth rate in coral literature has been replaced by appropriate terms like extension rate or calcification rate since sometime they do not show linear relationship. However in our case we use the term growth rate representing both extension rate and calcification rate since they show a strong correlation. Fig 3.18 shows this relation for the two tracks, Track-1(a) and Track-2 (b).

Next we show that the $\delta^{18}O$ profiles preserve the environmental parameters. Fig 3.19 shows the covariations between $\delta^{18}O$ and SST for Tr-1. The linear regression between these two parameters yield the following equations:

$$\delta^{18}O = (0.312\pm0.44) - (0.21\pm0.018)\ SST \quad \text{for Tr-1} \qquad (3.8)$$

r=–0.855, n=51, p=0.1, and

$$\delta^{18}O = (2.20\pm1.02) - (0.28\pm0.06)\ SST \quad \text{for Tr-2} \qquad (3.9)$$

r=-0.64, n=35, p=0.1.

The temperature coefficient (0.2±0.018) in Tr-1 is equal to that of the original palaeotemperature equation of Epstein *et al.* (1953). The temperature coefficient in Tr-2 (0.28±0.06) shows a little more scatter; however it also agrees with the equation of Epstein *et al.* (1953) within $\pm1\sigma$ uncertainty. The mean seasonal amplitude in SST in this region is ~5°C, whereas the observed SST variations from coralline the $\delta^{18}O$ is 3.5±1°C. In extreme cases they agree within $\pm1\sigma$ uncertainties. However a better agreement would

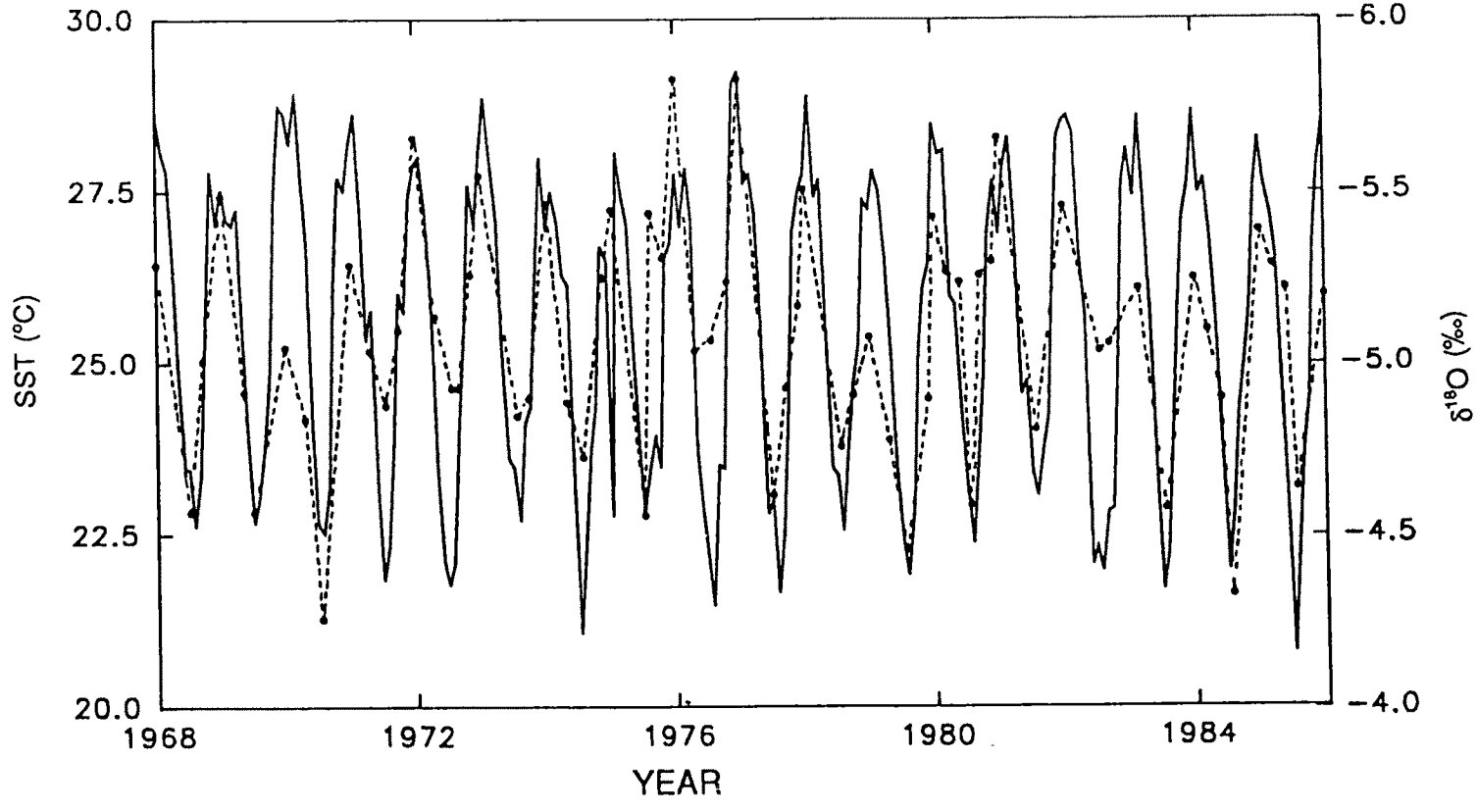

Fig 3.19 Covariation of SST and $\delta^{18}O$ of *Porites lutea* from the Stanley Reef, Australia. solid line: SST; dotted line:$\delta^{18}O$

have been possible with higher sampling resolution. Using the results of simulation presented in the previous section III.2.c we observe that for a ratio of $\Delta x/g = 0.27$ (typical for Tr-1) the $\delta^{18}O$ amplitude can reduce by 22%. When corrected for this reduction, the $\delta^{18}O$ amplitude translated to SST variations would yield a value of 4.35°C consistent (within $\pm 1\sigma$ errors) with the actual SST variations in this region. Considering the limitations of the model, as already discussed, we can expect this coral as a reliable SST recorder.

The $\delta^{18}O$ also shows a linear negative correlation with rainfall of Queensland coast. Regression analyses of this data yield the following Eqns:

$$\delta^{18}O = -4.65 - 0.002\ R \quad \text{for Tr-1} \qquad (3.10)$$

($r = -0.56$, $n=60$, $p=0.1$) and

$$\delta^{18}O = -4.62 - 0.002\ R \quad \text{for Tr-2} \qquad (3.11)$$

($r = -0.36$, $n=44$, $p=0.1$)

where R is the monthly rainfall in mm. In this we also see that Tr-1 is better correlated with rainfall than Tr-2. Our results are consistent with that of Aharon(1991) who shows that $\delta^{18}O$ in *Porites australiensis* from the Palm island (near to the Stanley Reef) is negatively correlated to the local precipitation. On the other hand carbon isotopic variations in this coral seem to be affected by the cloudiness; as was observed in corals from the Lakshadweep and the Gulf of Kutch. During Jan-Feb, the months of maximum cloud (Lough 1993) in the Queensland coast reduces the available light and hence the photosynthesis rate. This results in a reduction of $\delta^{13}C$ in coral $CaCO_3$. On a longer time scale, the $\delta^{13}C$ values show a decreasing trend. A factor contributing to this decreasing trend in $\delta^{13}C$ with time (Fig 3.21) seems to be related to the growth rate dependent fractionation; as was inferred for $\delta^{13}C$ data of the Kavaratti coral, KV-2. The coral shows a significant variability in its growth rate, 6-16mm/yr in Tr-1 and 10-16mm/yr in TR-2 (Fig 3.20). The decreasing trend in $\delta^{13}C$ in either of the track also explains that higher growth rate cause more fractionation in $\delta^{13}C$. Since the two tracks are close to each other, the variations in growth rate are expected to be the same which is evident from the near symmetric behaviour of the Fig 3.20. Small deviations from the symmetry is partly due to human error arising from the band thickness measurement from the X-ray picture, and partly due to the actual variations in growth rate in two tracks. The Fig 3.21 shows the

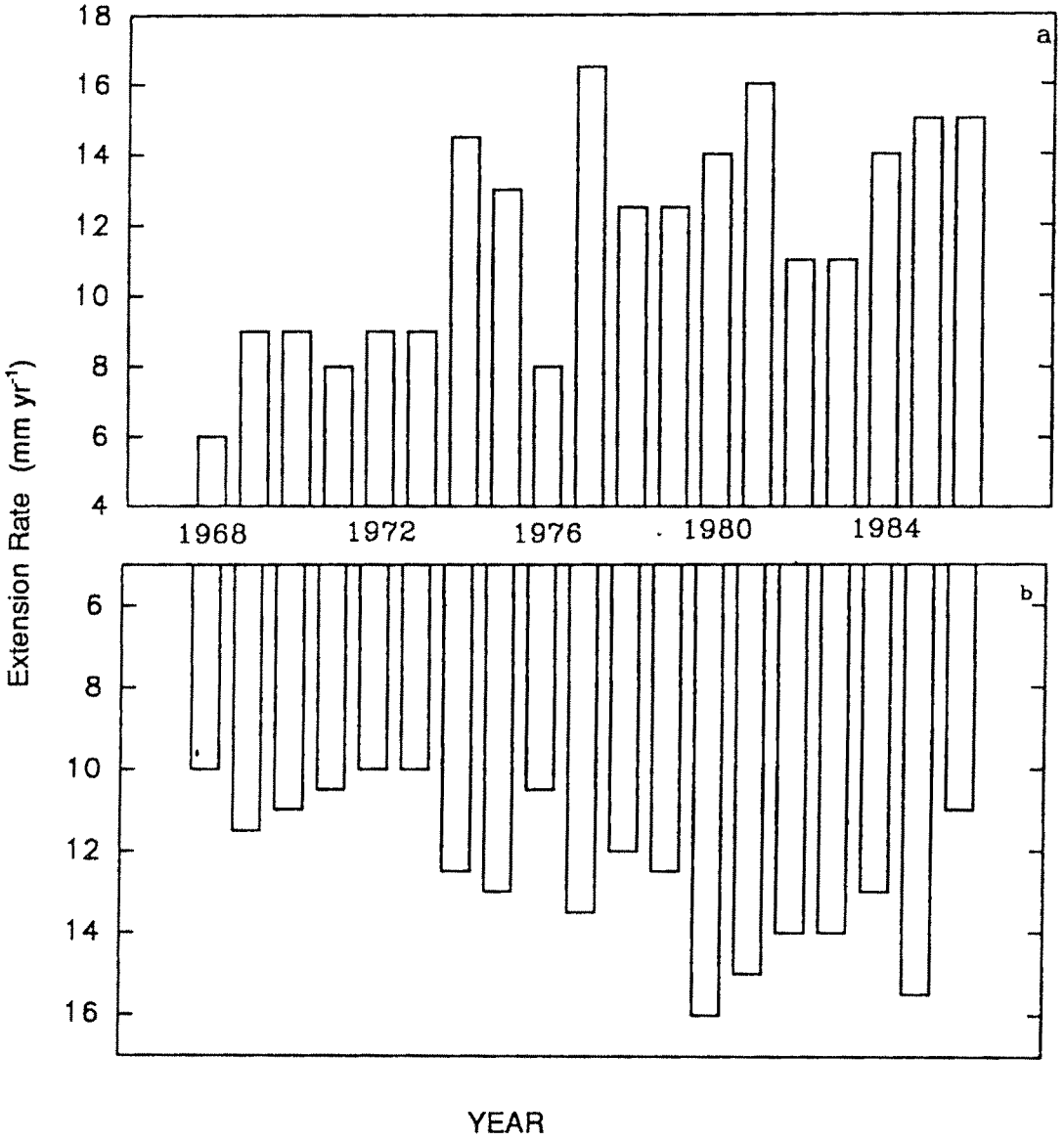

Fig 3.20 Growth rate variability in Track-1 and Track-2 of *P.lutea* from the Stanley Reef, Australia. (a) Track-1, (b) Track-2.

$\delta^{18}O$, $\delta^{13}C$ and density variations in Tr-1. And those of Tr-2 are presented in Fig 3.22.[Table III.8 in Appendix A].

The mean $\delta^{18}O$ of Tr-1 (no. of analysis n=67) is $-5.07\pm0.35‰$ and that of the Tr-2 (n=54) is $-4.97\pm0.39‰$. Similarly the mean $\delta^{13}C$ values are $0.95\pm0.38‰$ (Tr-1) and $-0.83\pm0.39‰$ (Tr-2). The mean densities for the two tracks are 1.47 ± 0.11 and 1.42 ± 0.21 respectively. Within the experimental uncertainties they are in good agreement. The variances in both the isotope ratios in both the tracks are remarkably similar. The smooth lines show the trends in various profiles obtained by fitting the fourth order polynomial. These exhibit the long term trends in the respective time profiles and also represent their resemblances.

Following a procedure of analysis of variance developed for tree rings as outlined by Fritts (1976), we calculate the common variances in the $\delta^{18}O$, $\delta^{13}C$ and density between the two tracks to be 67%, 54% and 68% respectively. This suggests that the intraband isotope variability introduces about 40% noise in the signal. Part of this "noise" could be an experimental artifact. That is, we have assumed that the pair of samples we analyzed from the same annual bands, along the two tracks were precipitated during the same time. In practice it is difficult to confirm this assumption, and errors could be introduced if the samples were precipitated a few weeks apart. This problem will be accentuated when samples are taken from narrow bands and when the samples represent climatic transition zones like winter to summer. Secondly, there could be genuine differences in the isotopic ratios as demonstrated by McConnaughey (1989), who showed progressive enrichment in $\delta^{13}C$ of the portion of the coral growing at a lower rate due to the deficiency of sunlight.

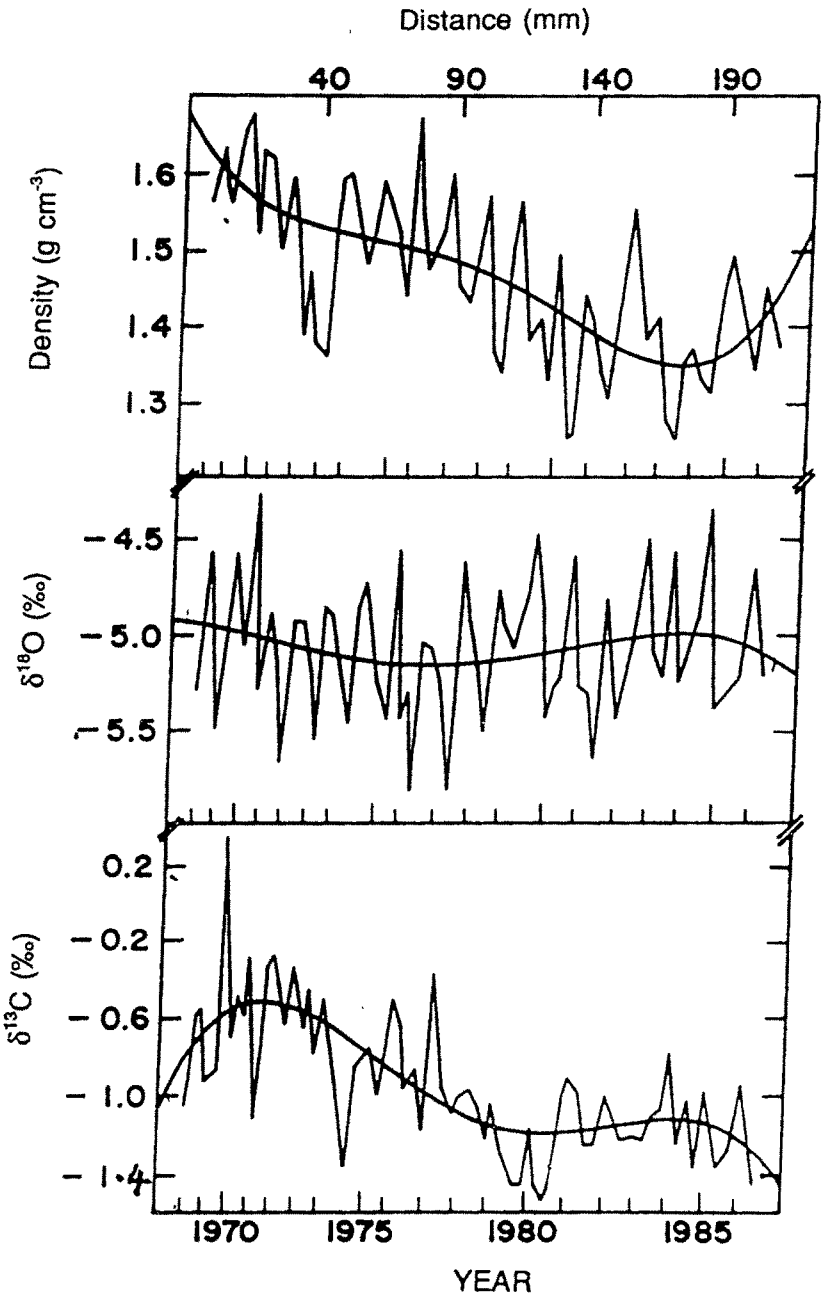

Fig 3.21 Density, $\delta^{18}O$ and $\delta^{13}C$ variations along Track-1 of coral *P. lutea* from Stanley Reef, Australia. Smooth lines indicate long term trends.

Table III.9 Correlation among the stable isotopes and the density variations.

	Linear correlation coefficient	
	actual data	detrended data
$\delta^{18}O$ & Density		
Track-1	0.23	0.29
Track-2	0.36	0.18
$\delta^{13}C$ & Density		
Track-1	0.56	0.20
Track-2	0.54	0.17
$\delta^{18}O$ & $\delta^{13}C$		
Track-1	0.02	0.04
Track-2	0.28	0.31

Table III.9 shows the linear correlation coefficients between $\delta^{18}O$ & density, $\delta^{13}C$ & density, $\delta^{18}O$ & $\delta^{13}C$ for the two tracks. There are long term trends in the records as shown by smooth lines in Figs 3.21, 3.22. The data have been detrended and the linear correlation coefficients are calculated for the detrended data. There is no significant correlation between $\delta^{18}O$ and density in either track, before or after detrending (Table III.9), suggesting that the density band variations are not controlled by SST variations. There is a significant correlation between $\delta^{13}C$ and density in each track before the data are detrended. This correlation becomes insignificant when the data are detrended. This has an important implication. As discussed earlier the decreasing trend in $\delta^{13}C$ is due to growth rate related fractionation. Hence if density correlates with $\delta^{13}C$ but not with $\delta^{18}O$ it implies that the density band formation takes place due to the changes in the growth rate rather than SST. The decreasing trend in $\delta^{13}C$ is due to the variable growth rate as discussed. Hence detrended profile effectively shows the carbon isotopic variations due to an external factor, like photosynthesis which is governed by availability of sunlight. The lack of a significant correlation between density and $\delta^{13}C$ (after detrending) probably implies that density band formation is more influenced by endogenic rather than exogenic factors.

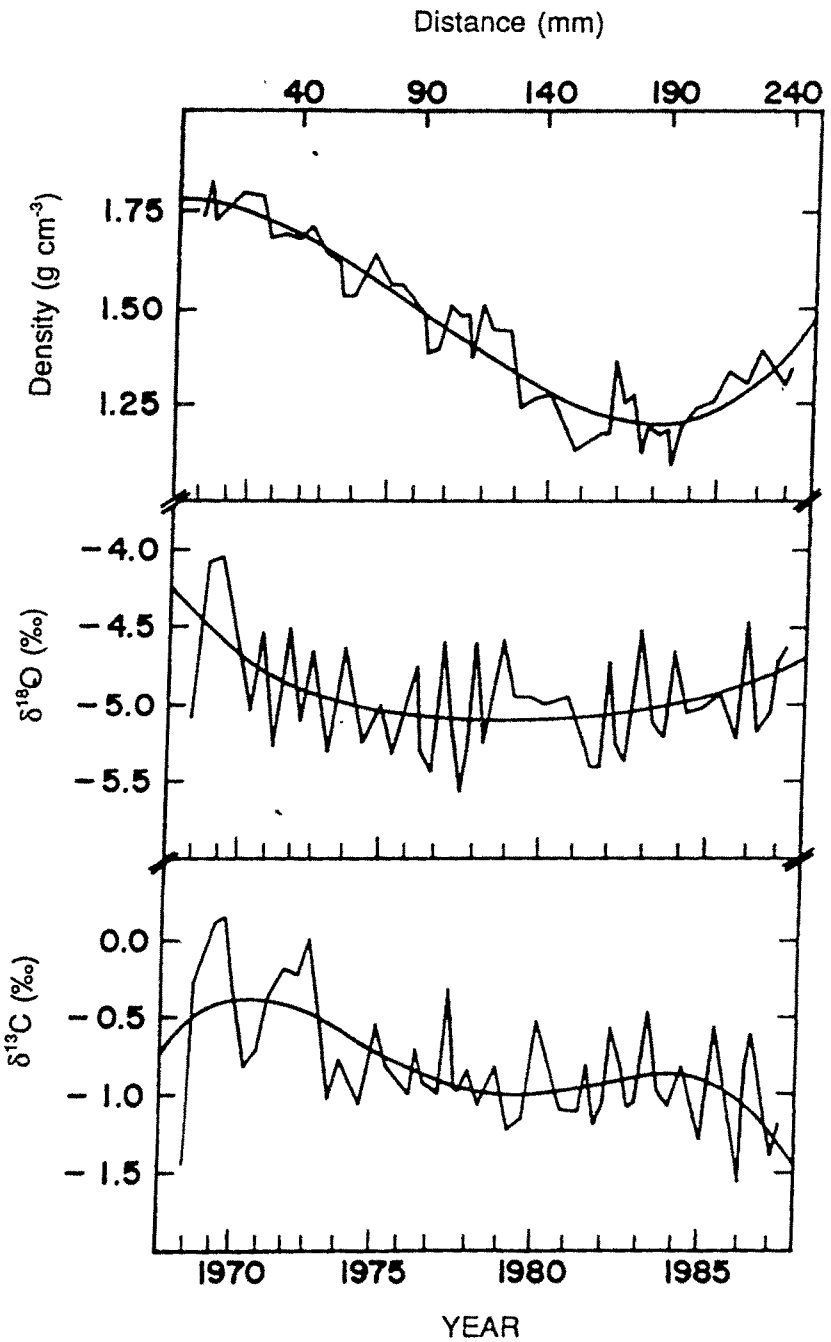

Fig 3.22 Density, $\delta^{18}O$ and $\delta^{13}C$ variations along Track-2 of coral *P. lutea* from the Stanley Reef, Australia. Smooth lines indicate long term trends.

The corals in this region generally acrete high density bands in summer and low density bands in winter. Lough & Barnes(1991) made detailed investigation on this aspect. The coral density decreases with time in both the tracks (Figs 3.21 & 3.22). The magnitude is about 0.25 g/cm^3 for track 1 and 0.5 g/cm^3 for track 2 between 1968 and 1984 A.D. The reduction in density is more pronounced in the track which is farther away from the central growth axis. The $\delta^{13}C$ also decreases by 0.5‰ in both the tracks during this period. The positive correlation between $\delta^{13}C$ and density in each of these tracks, therefore, arises due to the long term trend in the data. Slower growth rate corresponds to higher density as seen in the above figure and during 1968-74, the early part of the record. The later part of the record shows higher growth rates and lower densities in general. As shown by McConnaughey (1989), the $\delta^{13}C$ values in years of slow growth are isotopically enriched compared to those of years of higher growth rate. Therefore we infer that the density banding is more likely to be determined by variation in growth and rather than by variations in SST. This is to some extent corroborated by the fact that $\delta^{18}O$ and $\delta^{13}C$ are not correlated. If the kinetic effects were dominant during the fractionation of the isotopes from the sea water to the coral skeleton, one would observe a strong positive correlation between the $\delta^{18}O$ and $\delta^{13}C$ (McConnaughey 1989). The absence of such a correlation also indicates that metabolic (growth related) fractionation is dominant in the case of $\delta^{13}C$.

Density, $\delta^{18}O$ and $\delta^{13}C$ time series obtained from two tracks of a *Porites* coral, one close to growth axis (10° off) and another 20° off the axis indicate that there is a small but systematic intraband variability across the central growth axis. Oxygen isotopic ratio, an indicator of the environmental parameter shows a good correlation with SST in both the tracks, however the correlation is weaker in the track 20° off the growth axcis. A similar trend is also observed in case if $\delta^{18}O$-rainfall correlation. The carbon isotopic composition seems to be largely controlled by intrinsic factors like metabolism and the variable growth rate. The correlation between density and $\delta^{13}C$ implies that the density band formation is controlled more by variable growth rate rather than SST.

III.3 RADIOCARBON RESULTS

The primary goal of measuring radiocarbon in the Gulf of Kutch coral is to determine the air-sea CO_2 exchange rate (ASCER) in this region. The ^{14}C concentrations in the atmosphere and upper layers of the ocean were significantly perturbed by nuclear weapon tests conducted during the 1950's and early 60's. (de Vries 1958, Levin *et al.* 1980) This perturbation and its temporal variation provides a means to determine the ASCER in different regions of the ocean (Broecker *et al.* 1980, Stuiver 1980, Druffel & Suess 1983, Siegenthaler 1983, Cember 1989, Weidman & Jones 1993).

The ASCER can be derived by modelling the temporal variations in ^{14}C activities of the atmosphere and the surface ocean. The time variations in the surface ocean radiocarbon is derived from ^{14}C measurements in the annual growth bands of coral; tree rings provide the radiocarbon time history of the atmosphere. With this objective we have measured radiocarbon in the annual bands of corals and tree rings.

Features of the data

III.3.a Gulf of Kutch coral

Fig 3.23 shows the $\Delta^{14}C$ time-series in the Gulf of Kutch (GKh, 22.6° N, 70° E) coral for the years 1950-1990 [data in Table III.12, Appendix A]. From a value of -60‰ in the year 1950 it steadily increases to a peak value of 170‰ in 1968, after which it decreases monotonically to a value of 55‰ in 1990. The increase in ^{14}C activity since 1950 results from the injection of bomb produced radiocarbon from the atmosphere to the surface ocean via air-sea CO_2 exchange. Moore and Krishnaswami (1974) had reported $\delta^{14}C$ time series for a *Favia* coral in the GKh for the years 1951 to 1973. They obtained a peak value of +230‰ for $\delta^{14}C$ in 1968. This $\delta^{14}C$ when corrected for isotopic fractionation using a $\delta^{13}C$ value of -0.27‰ (our measured value in the GKh coral) yields a $\Delta^{14}C$ of 169‰ very close to the peak value of 170‰ obtained in this study.

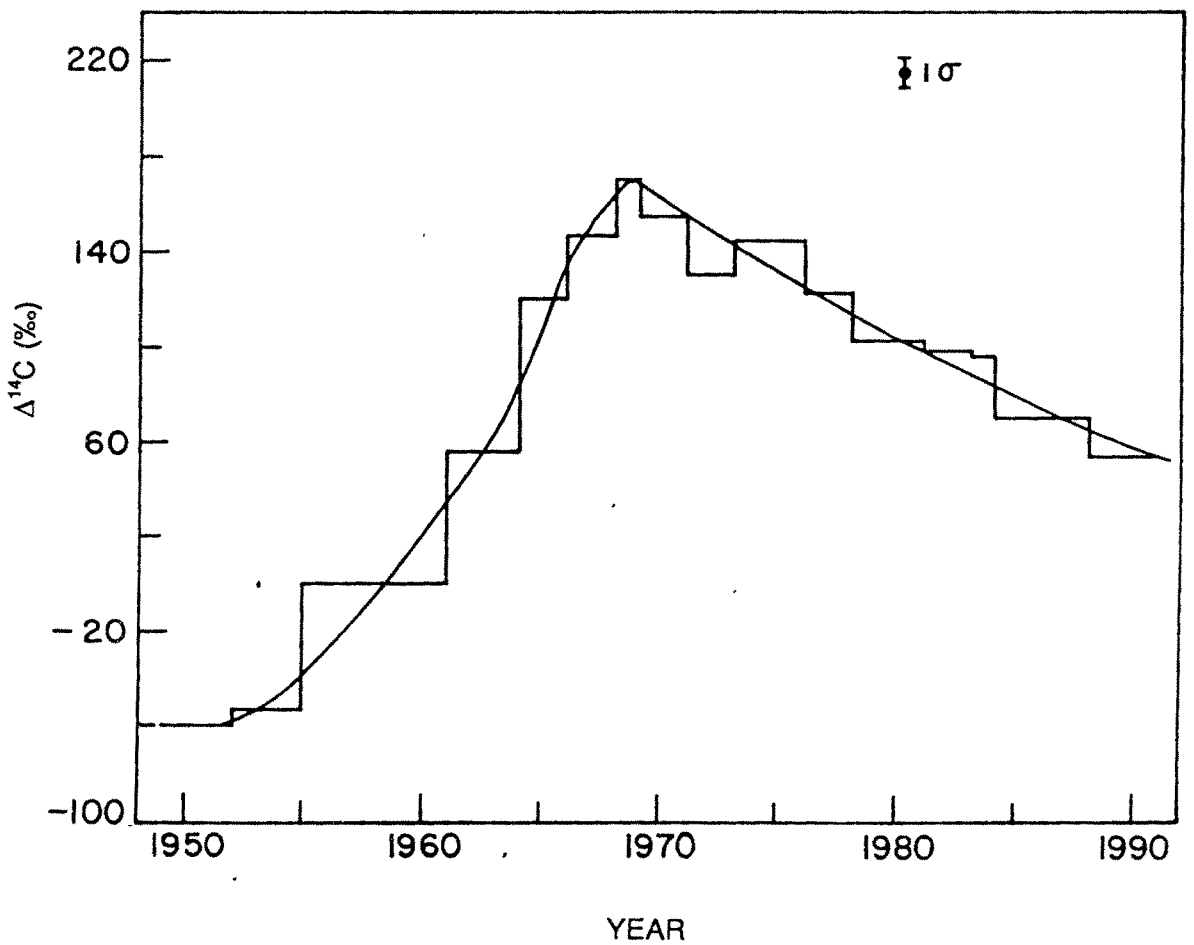

Fig 3.23 $\Delta^{14}C$ time series in the coral *F. speciosa* from the Gulf of Kutch, northern Arabian Sea. The continuous curve is an eye fit line to the data.

III.3.b Tree rings

The $\Delta^{14}C$ time profile in the annual rings of a teak tree from Thane (19°14'N,73°24'E, about 25 km north of Bombay) is shown in Fig 3.24 [data in Table III.12 Appendix A] along with the northern hemispheric (NH) curve (Nydal & Lövseth 1983, Gupta & Polach 1985). The Thane tree ring samples we analyzed cover a time span of 1960 to 1980. In the early sixties, the $\Delta^{14}C$ values of the Thane tree rings are indistinguishable from that of NH values, but the two sets of values differ significantly after mid sixties through the year 1980. The Thane tree ring $\Delta^{14}C$ reaches a peak value (630‰) during 1964-65, significantly lower than that of the NH peak of ~1000‰ Radiocarbon analyses of air samples from Bombay during 1963-64 (Kusumgar 1965) also show that the $\Delta^{14}C$ of Bombay air (~700‰) is similar to the tree ring value but lower than that of the NH curve. Broecker *et al.* (1985) give 3 curves for atmospheric $\Delta^{14}C$ time series for the regions: >20°N, 20°N-20°S, and >20°S. The tree analyzed in this study (located at 19°N) belongs to the middle group, its peak $\Delta^{14}C$ value is ~100‰ less compared to that expected from the 20°N-20°S curve. We need to obtain better spatial coverage of tree ring $\Delta^{14}C$ data for this region to ascertain the observed lower $\Delta^{14}C$ values. If the $\Delta^{14}C$ in this region is indeed lower, it could arise from:

1) local dilution of ^{14}C activity of this region. Kusumgar (1965) attributed the lower $\Delta^{14}C$ in Bombay air relative to northern hemispheric values to fossil fuel injection of CO_2.

2) active air-sea exchange of CO_2 with the adjoining Arabian Sea. The evasion of CO_2 depleted in ^{14}C from the Arabian Sea may reduce the $\Delta^{14}C$ peak in the atmosphere.

Another reason of reduced peak in the Thane region compared with the NH peak could be the enhanced mixing between stratosphere and troposphere, which result in higher ^{14}C concentration in the high latitudes relative to that in the lower latitudes (Hagemann *et al.* 1965).

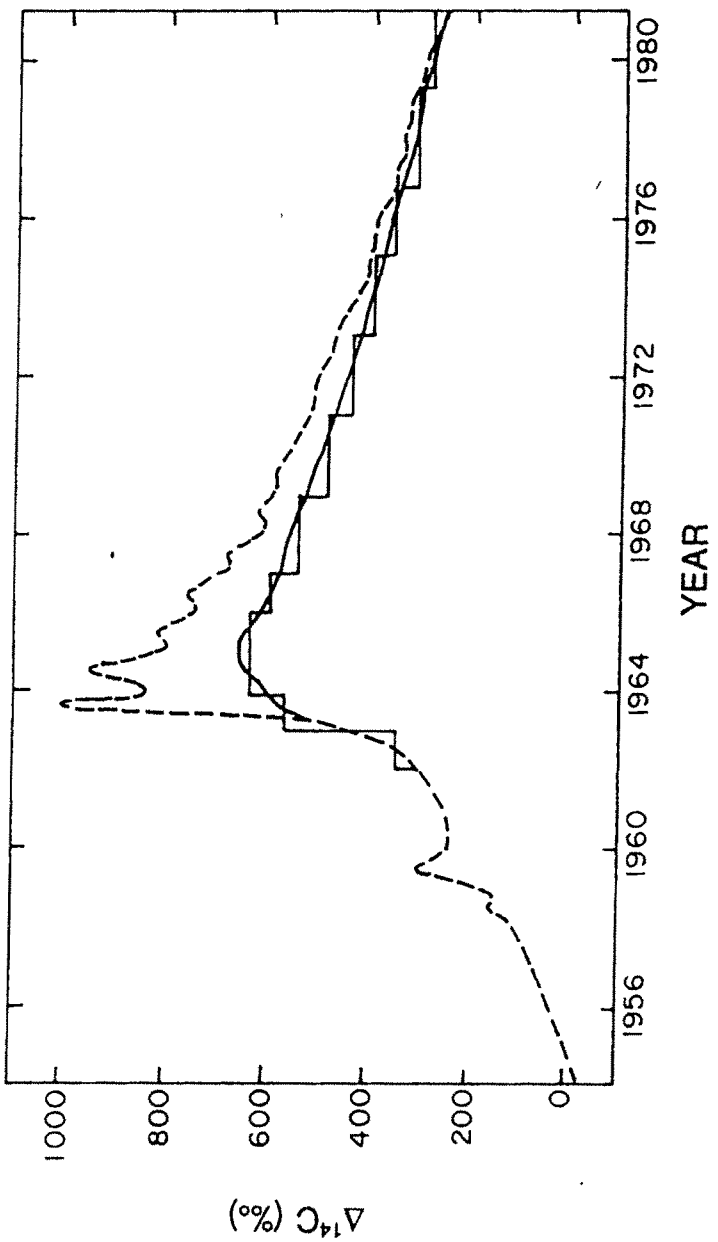

Fig 3.24 Atmospheric $\Delta^{14}C$ time variations of the Northern Hemisphere (long dashed line, data from Nydal & Lövseth 1983) and Thane (near Bombay, solid line). The Thane data are based on tree ring measurements. The Thane values are significantly lower than the NH curve. Error bar is too small to be shown.

III.3.c Air-Sea CO_2 exchange rate (ASCER) in the Gulf of Kutch

Comparison of the $\Delta^{14}C$ time series of the coral (representative of surface sea water) and that of the tree ring (atmosphere) shows that $\Delta^{14}C$ peak in the GKh coral lags behind the atmospheric peak by 4-5 years. This "peak shift" provides information about the CO_2 exchange time scales between the atmosphere and ocean in a particular oceanic region, and is related to the residence time of CO_2 in atmosphere wrt the exchange with the ocean as discussed later. The peak-shift for other oceanic regions range between 4-15 years (Table.III.10). The 4-5 years response time in the GKh region probably indicates that the ASCER is greater in this region, resulting from strong monsoon winds.

Model for calculation of ASCER

Determination of the CO_2 exchange rate between atmosphere and the surface ocean requires a knowledge of sources and sinks of carbon and radiocarbon in the particular oceanic region. The carbon budget in surface water is controlled mainly by air-sea CO_2 exchange, advective processes (lateral and/or vertical mixing of water masses) and biological productivity. The Gulf of Kutch area is a shallow continental shelf region having mean water depth of ~30 m. The GKh exchanges water with the adjoining Arabian Sea through tidal currents. The speeds of these currents vary from 0.5 to 0.76 m/sec (Srivastava & John 1977). The mass balance equations for ^{12}C and ^{14}C in the Gulf of Kutch between supply and removal is given by:

$$\begin{bmatrix} \text{invasion of } CO_2 + \\ \text{advective transport} \end{bmatrix} = \begin{bmatrix} \text{evasion of } CO_2 \quad + \quad \text{advective transport} \\ + \qquad \text{biological} \quad \text{removal} \end{bmatrix}$$

For ^{12}C this is given by (assuming invasion and evasion of CO_2 are equal)

$$F_{12} + w\,C_S = F_{12} + w\,C_G + B \qquad (3.12)$$

$$w\,C_S = B + w\,C_G \qquad (3.13)$$

Table: III.10 $\Delta^{14}C$ minimum, maximum and peak shift for different oceanic regions. The minima of $\Delta^{14}C_{coral}$ represent the pre-bomb values. The time difference between the peaks in $\Delta^{14}C$ of the atmosphere and the coral (surface ocean) is termed "peak shift". The atmospheric peak was taken to be in the year 1963.

Oceanic region	$\Delta^{14}C_{coral}$ min	max	Year of maximum	Peak Shift (yr)	Reference
Bermuda 32°N, 65°W	-50	168	1975	12	Nozaki *et al.* 1978
Florida 24°57'N 88°33'W	-55	160	1972	9	Druffel & Linik 1978
Oahu 21°N, 158°W	-	175	1973	10	Toggweiler *et al.* 1991
Belize 16°50'N 83°48'W	-55	160	1972	9	Druffel 1980
North Red Sea 12°N,43°E	-75	105	1967	4	Cember 1989
South Red Sea 11.5°N, 43°E	-73	~45	1972	>7	Cember 1989
Tarawa 1°N, 172°E	-	103	1978	15	Toggweiler *et al.* 1991
Galapagos 1°S, 90°W	-72	25	1973	10	Druffel 1981
Fiji 18°S, 179°E	-70	138	1974	11	Toggweiler *et al.* 1991
Tonga 20°S, 175°W	-	157	1975	12	Toggweiler *et al.* 1991
Gulf of Kutch 22.6°N, 70°E	-65	172	1968	5	This work

where F (mol m^{-2} yr^{-1}) is the CO_2 exchange flux, w (m yr^{-1}) advection velocity, C (mol m^{-3}) carbon concentration and B (mol m^{-2} yr^{-1}) is biological removal. The subscripts S and G refer to the surface Arabian Sea and the Gulf of Kutch respectively. The above equations assume steady state for ^{12}C balance. . This assumption is an oversimplification as the CO_2 concentration of atmosphere has been steadily increasing during the past century (Bacastow & Keeling 1981, Siegenthaler & Sarmiento 1993) which would affect the invasion-evasion balance.

The mass balance equation for ^{14}C is of the following form (neglecting radiocarbon decay, see Appendix-I).

$$D_G \frac{dC_G^*}{dt} = F_{12}(R_A - R_G) + w(C_S R_S - C_G R_G) \qquad (3.14)$$

where R is the $^{14}C/^{12}C$ mol ratio in the respective reservoir. Subscripts A and G stand for the atmosphere and GKh respectively. C_G^* is the radiocarbon concentration in GKh and D_G is the mean depth of GKh (Table III.11). The formulation of our model is similar to that used by Cember (1989) for deriving ASCER in the Red Sea region. Eqn 3.14 can be written in the standard $\Delta^{14}C$ notation. The first term in the RHS, the net ^{14}C flux, ΔF_{14}, between the atmosphere and the GKh can be expressed as (Stuiver 1980):

$$\Delta F_{12} = k(\Delta^{14}C_A - \Delta^{14}C_G)F_{12} \qquad (3.15)$$

where k is a factor which takes into consideration the $^{14}C/^{12}C$ mol ratio of the NBS oxalic acid standard (1.176×10^{-12}) and fractionation factor for the inter-reservoir carbon transfer. The numerical value of k is 1.24×10^{-15} (*op cit.*). $\Delta^{14}C_A$ and $\Delta^{14}C_G$ are the atmospheric and GKh radiocarbon activities. The second term in the RHS (Eqn 3.14) represents the exchange flux of radiocarbon between the Arabian Sea and GKh by advection. This term can be written as:

$$F_{CG} = u[m(\Sigma CO_2)_S(1 + \frac{\Delta^{14}C_S}{1000}) - m(\Sigma CO_2)_G(1 + \frac{\Delta^{14}C_G}{1000})] \qquad (3.16)$$

where m is a constant which is obtained by multiplying the $^{14}C/^{12}C$ mol ratio of the NBS

Oxalic acid standard and the fractionation term for transfer of carbon between different reservoirs. That is, m=(1.176x10^{-12}x1.052)=1.24 x 10^{-12} [vide Appendix II]. The solution of the Eqn 3.14 is given by:

$$\Delta^{14}C_G(t) = \Delta^{14}C_G^o e^{-Jt} + Ee^{-Jt}\int_o^t e^{Jt}\Delta^{14}C_A(\tau)d\tau + Fe^{-Jt}\int_o^t e^{Jt}\Delta^{14}C_S(\tau)d\tau \qquad (3.17)$$

where $\Delta^{14}C_G^o$ is the initial value (pre-bomb) of $\Delta^{14}C$ in GKh, J, E and F are constants (Appendix-III). The values of various parameters used in this model are given in Table III.11.

As a first step we calculate $\Delta^{14}C_G(t)$ using Eqn 3.17 with two simplifications, (i) $[\Sigma CO_2]_S = [\Sigma CO_2]_G$ and (ii) the advective transport process is negligible, *i.e.* the ^{14}C time variations in the GKh is controlled only by carbon exchange with the atmosphere. Druffel & Suess (1983) also modelled their ^{14}C data in corals from north-west Atlantic and eastern tropical Pacific to derive exchange time scales and CO_2 exchange rate based on a similar simplified model. Eqn 3.14 with w=0 reduces to the model used by Druffel & Suess (1983) *i.e.* the time variations of ^{14}C concentration in sea surface water is proportional to the air-sea gradient of $\Delta^{14}C$.

Solving Eqn 3.17 with w=0 and for different F_{12} values we obtain a family of curves (Fig 3.25). The curve (a) with F_{12} =2 shows that the GKh radiocarbon activity increases monotonically through 1980 without a distinct peak. This is not consistent with our coral data (filled circle in Fig 3.25) which show a distinct peak in 1968. The second and third curves (b) and (c) with F_{12} =6 and 10 respectively, though show peaks in the $\Delta^{14}C$ time series, they predict much higher radiocarbon concentration in the GKh compared to that observed in the coral. It is clear from these results that the air-sea exchange alone is not able to simulate the observed $\Delta^{14}C$ variations in the GKh coral. Therefore carbon and radiocarbon supply to the GKh via advection from the Arabian Sea also need to be considered, which would 'dilute' the effects of air-sea exchange and thereby provide a better fit to the coral data.

The advective supply of carbon to the GKh could be from the surface layer or shallow depths of the Arabian Sea. Solution of Eqn 3.17 requires knowledge of time

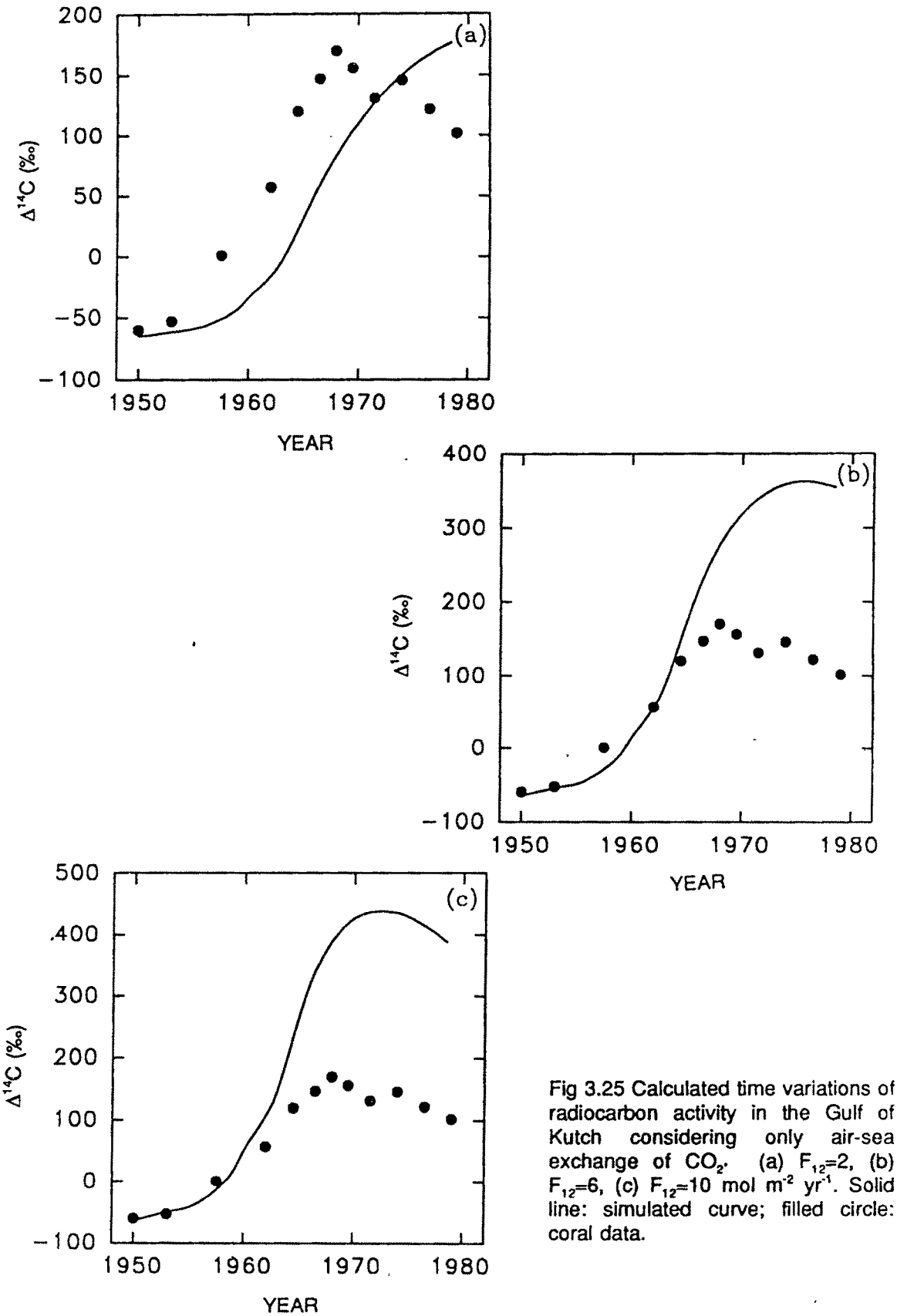

Fig 3.25 Calculated time variations of radiocarbon activity in the Gulf of Kutch considering only air-sea exchange of CO_2. (a) F_{12}=2, (b) F_{12}=6, (c) F_{12}=10 mol m^{-2} yr^{-1}. Solid line: simulated curve; filled circle: coral data.

Table III.11 Symbols, units and values of parameters used in our model

Symbol	Parameter	Unit	Value	Reference
F_{12}	air-sea exchange rate of CO_2	mol $m^{-2}yr^{-1}$	model derived	
C_S, $(\Sigma CO_2)_S$	total DIC conc. in surface Arab. Sea	mol m^{-3}	2.11	Stuiver & Östlund 1983
C_D, $(\Sigma CO_2)_D$	total DIC conc. of deep Arab. Sea	mol m^{-3}	2.36	-do-
C_G, $(\Sigma CO_2)_G$	total DIC conc. in GKh	mol m^{-3}	2.11	-do-
R	$^{14}C/^{12}C$ mol ratio	-	variable	
C^*	radiocarbon conc.	mol m^{-3}	variable	
D_S	mixed layer depth of Arab. Sea	m	60	
D_G	mean depth of GKh	m	30	
$(\Delta^{14}C)_A^\circ$	Pre-bomb atmospheric $\Delta^{14}C$	‰	-25	Stuiver & Quay 1981
u	upwelling velocity	m yr^{-1}	model derived	
w	advective velocity Arab. Sea to GKh	m yr^{-1}	model derived	

variations in R_S, the Arabian sea water contributing radiocarbon to GKh. Since there is no data on $\Delta^{14}C$ time series of the surface Arabian Sea, we need to generate the same for the time period 1953 to 1980, based on input from atmosphere and upwelling from the deep Arabian Sea. We constrain this time series with the 1977 mixed layer $\Delta^{14}C$ value of 59‰ based on the GEOSECS (station 416) measurements. We consider the following two box model for the Arabian Sea consisting of surface and deep layers (Fig 3.26).

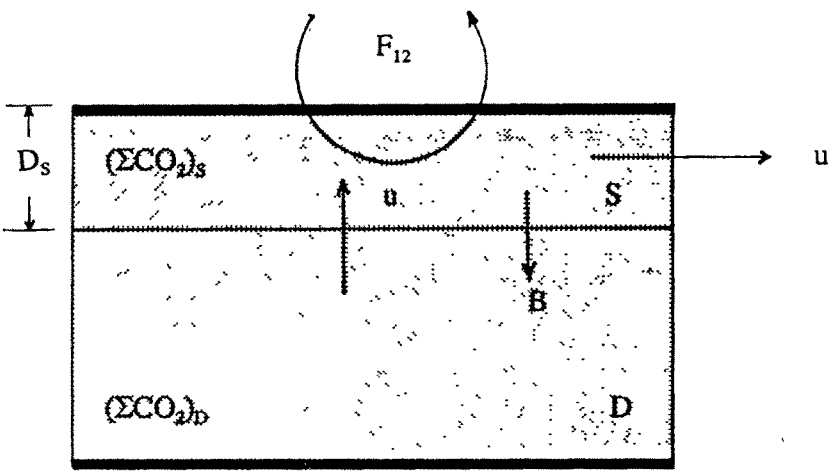

Fig 3.26 Two box model of the (northern) Arabian Sea. S is mixed layer, D is deep ocean, other parameters are defined in Table III.11

The mass balance equation for ^{14}C for the mixed layer is given by:

$$D_S\frac{dC_S^*}{dt} = F_{12}R_A + uC_DR_D - (uC_SR_S + BR_S + F_{12}R_S + \lambda C_SR_SD_S) \qquad (3.18)$$

Neglecting the decay term and substituting, $uC_D=B+uC_S$ (*cf.* Eqn 3.13) we get:

$$D_S \frac{dC_S^*}{dt} = F_{12}(R_A - R_S) + u(C_D R_D - C_D R_S) \qquad (3.19)$$

Rewriting in terms of $\Delta^{14}C$ (*c.f.* Eqns 3.15 & 3.16),

$$D_S(\Sigma CO_2)k\frac{d\Delta^{14}C_S}{dt} = F_{12}k(\Delta^{14}C_A - \Delta^{14}C_S) + u(\Sigma CO_2)_D m(\frac{\Delta^{14}C_D}{1000} - \frac{\Delta^{14}C_S}{1000}) \qquad (3.20)$$

Eqn 3.20 has a solution of the form:

$$\Delta^{14}C_S(t) = e^{-At}\Delta^{14}C_S^o + Be^{-At}\int_o^t e^{At}\Delta^{14}C_A(\tau)d\tau + \frac{C}{A}(1 - e^{-At}) \qquad (3.21)$$

where A,B, and C are constants (Appendix IV).

Using Eqn 3.21 we generate mixed layer Arabian Sea $\Delta^{14}C$ time series based on the atmospheric $\Delta^{14}C$ values. The atmospheric $\Delta^{14}C$ values for 1950-1960 were taken from Stuiver & Quay (1981) and Gupta & Polach (1985). For 1960-1980, the Thane tree ring $\Delta^{14}C$ (Fig 3.21) data were used. The deepwater $\Delta^{14}C$ end member value used was -90‰ corresponding to that measured at a depth of ~500 m at GEOSECS station 416 (Stuiver & Östlund 1983). The time series is constrained by fixing the Arabian Sea mixed layer $\Delta^{14}C$ value as 59‰ for 1977(*op cit.*) and by the fact that the $\Delta^{14}C_{max}$ should occur around 1968. Typical results for the Arabian Sea time series are given in Fig 3.27. Reasonable estimates for F_{12} and u are:

$$F_{12} = 11 \text{ mol m}^{-2} \text{ yr}^{-1} \qquad \text{and} \qquad u = 10.5 \text{ m yr}^{-1}$$

These values though not unique (as they depend on the $\Delta^{14}C$ of the deep water end member used for calculations), they are consistent with other independent estimates.

(i) Broecker *et al.* (1985) has calculated the inventory of bomb ^{14}C in stn 416 to be 5.1×10^9 atom cm^{-2}. According to Stuiver (1980) the inventory is related to the CO_2 air-sea exchange flux as:

$$Q = 1.24 \times 10^{-15} F_{12} \int (\Delta^{14}C_A - \Delta^{14}C_S - 45)dt$$

The value of the integral between 1953-1977 is ~5500 ‰.yr based on our model derived

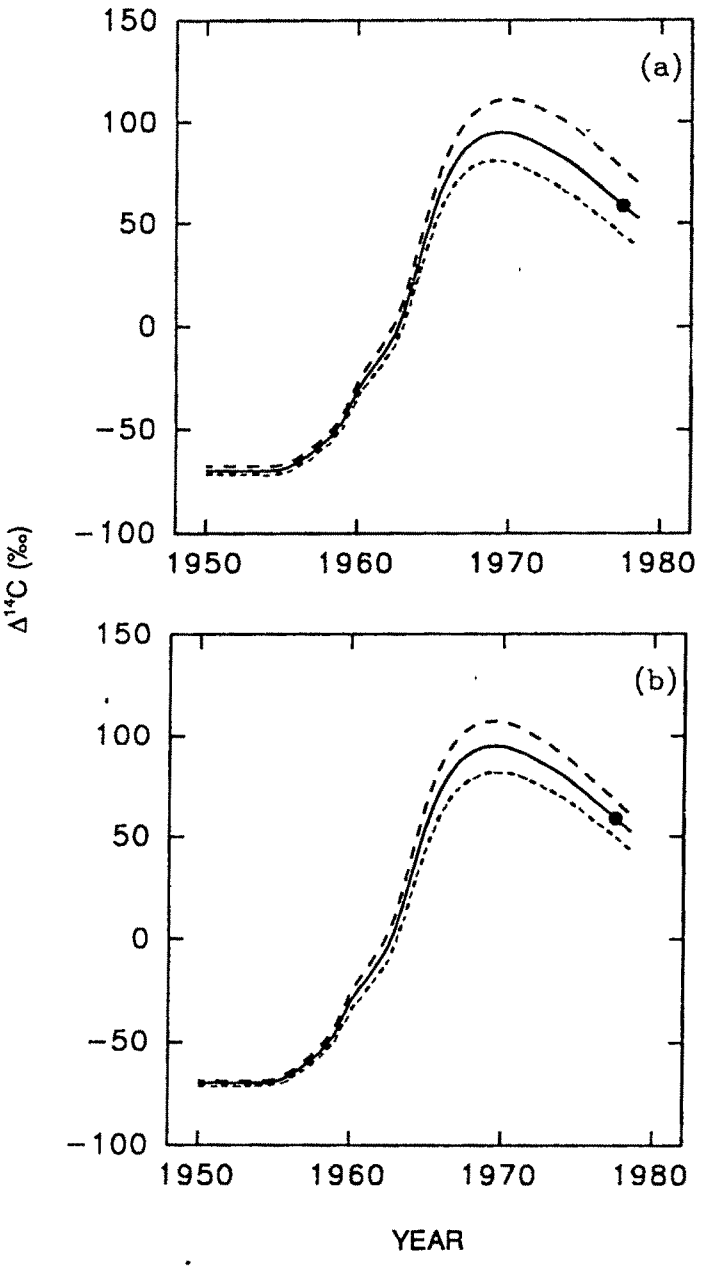

Fig 3.27 Results of box model calculation. The plots show the simulated radiocarbon time series in the mixed layer of the northern Arabian Sea (GEOSECS stn 416) for different sets of parameters. (a) constant F_{12} (11= mol m^{-2} yr^{-1}) and varying u (=9, 10.5, 12 m yr^{-1}), (b) constant u (=10.5) and varying F_{12} (=12, 11, 10). The filled circles represent the 1977 GEOSECS mixed layer $\Delta^{14}C$ value (59‰, Stuiver & Östlund 1983). Values of F_{12}=11 and u=10.5 (solid line) appears to be the best (eye) fit curve.

$\Delta^{14}C$ values of the surface Arabian Sea, atmospheric $\Delta^{14}C$ values used in this model, and a steady state $\Delta^{14}C$ difference between atmosphere and ocean of about 45‰. This yields a value of F_{12} = 12 similar to that derived using our model.

(ii) the mean annual wind speed in the northern Arabian Sea is about 6 m/s (Esbensen & Kushnir 1981). For this wind speed the expected CO_2 invasion flux is ~13 mol $m^{-2}yr^{-1}$ using the relationship between windspeed and CO_2 invasion flux (Broecker *et al.* 1985). Our calculation is in good agreement with this estimate.

(iii) Hasternath & Lamb (1980) estimated the upwelling velocity over the whole of the Arabian Sea and the Bay of Bengal from 200 m depth to be ~ 19 m yr^{-1}. Warren (1992) reports the mean upwelling rate into the bottom of the North Indian Deep Water layer ~ 15-30 m yr^{-1}; net upwelling out of the top of the layer to be less than this. Our calculation, the upwelling rate 10.5 m yr^{-1} from a depth of ~500m is not inconsistent with the above estimates.

(iv) the model derived steady state pre-bomb $\Delta^{14}C$ value for the surface Arabian Sea is

$$(\Delta^{14}C_S)_o = \frac{\Delta^{14}C_D u(\Sigma CO_2)_D + F_{12}(\Delta^{14}C_A)_o}{F_{12} + u(\Sigma CO_2)_D} = -70\ ‰$$

with u =10.5 and F_{12}= 11 the value (-70‰) is close to the number -65‰ used by Broecker *et al.* (1985) for the calculation of the bomb ^{14}C inventory in the station 416.

In addition, other consistency checks on the model can also be made by the following approximations. When F_{12}=0 atmospheric exchange is cut off) the $\Delta^{14}C_S$ approaches $\Delta^{14}C_D$ with a time constant of A^{-1} [Appendix IV] of 5 yrs. This implies that if the atmospheric exchange is cut off the mixed layer $\Delta^{14}C$ will become equal to that of the deep water in about 20-25 years (*i.e.* 4-5 times A^{-1}). Similarly for u=0 (*i.e.* no upwelling) $\Delta^{14}C_S$ approaches $\Delta^{14}C_A$ with a time constant of about 12 yrs. These time constants are similar to those observed for other oceanic regions for the residence time of carbon in the mixed layer wrt exchange with deep water and the atmosphere.

Now we use the Arabian Sea and the atmospheric $\Delta^{14}C$ time series as the two end members contributing carbon and radiocarbon to GKh to generate the $\Delta^{14}C$ time series in the Gulf of Kutch; [assuming that the DIC concentrations in these two reservoirs are

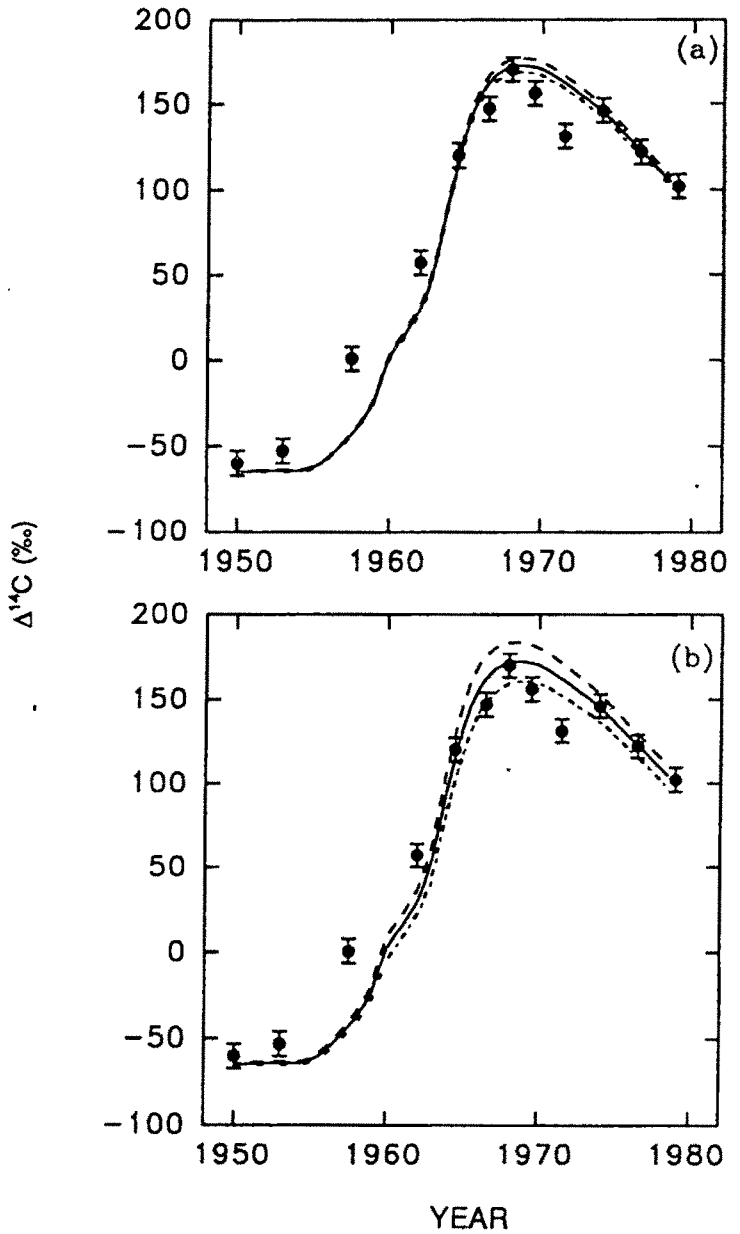

Fig 3.28 Results of box model calculations. The plots show the simulated radiocarbon time series in the Gulf of Kutch (GKh) for different sets of parameters. (a) constant F_{12} (=12 mol m^{-2} yr^{-1}) and varying w (=26, 28, 30 m yr^{-1}) and (b) constant w (=28) and varying F_{12} (=14, 12, 10). Filled circles represent GKh coral data with ±1σ errors. Values of F_{12} =12 and w = 28 (solid line) appear to fit the coral data reasonably well.

equal *i.e.* the biology term B=0, vide Appendix V], we generate a family of curves for different sets of values of F_{12} and w (Fig 3.28). The solid line is the calculated $\Delta^{14}C$ time series for the Gulf of Kutch, filled circles are our coral data.

It is seen from Fig 3.28 that the rise in $\Delta^{14}C$ of coral during 1953-1960 is faster than that predicted by the model. A factor which would have contributed to this is an averaging effect. The $\Delta^{14}C$ plotted for the year 1957.5 is an average for five coral bands 1955-1960. The steady increase in $\Delta^{14}C_A$ during these years is not considered in plotting this data point. Another cause for the discrepancy between the observed $\Delta^{14}C$ and the model fit, can be an error in the year assignment for the bands. As we have taken utmost care in sampling and verified the year assignments with the $\delta^{18}O$ data this error is unlikely, however, if at all there is an error it is likely to be ±1 yr.

The nature of curves in Fig 3.28 shows that the year of $\Delta^{14}C$ peak in the GKh is controlled more by F_{12}, whereas both F_{12} and w seem to influence the magnitude of the $\Delta^{14}C$ peak.

A reasonable fit to the coral data can be made using the values of

$$F_{12} = 12 \text{ mol m}^{-2} \text{ yr}^{-1} \quad \text{and} \quad w = 28 \text{ m yr}^{-1}$$

based on the $\Delta^{14}C$ time series of the two end members considered. In this case when $F_{12}=0$ the $\Delta^{14}C_G$ approaches $\Delta^{14}C_S$ with a time constant of ~1 yr and when w=0 the $\Delta^{14}C_G$ approaches to that of atmospheric activity with a time constant of about 5 yrs. As already mentioned that the peak shift obtained in our case 4 to 5 yrs is equivalent to this time constant, *i.e.* the residence time of the atmospheric carbon dioxide wrt the exchange between atmosphere and the GKh water when the GKh becomes isolated from the open ocean.

If the $\Delta^{14}C$ values of the Arabian Sea end member contributing radiocarbon to GKh is different from that used in the above model, then the values F_{12} and w for GKh would also differ correspondingly. There are no reported results on the circulation and hydrographic properties of the GKh and hence it is difficult at present to constrain our model further.

Our estimate of the CO_2 exchange rate 11-12 mol m^{-2} yr^{-1} in this region is in good agreement to that obtained from other investigations elsewhere. The upwelling in the northern Arabian Sea is calculated as 10.5 m.yr^{-1} and the Gulf of Kutch and

the Arabian Sea exchange water with each other with an annual mean flow of water mass 40 million cubic metre. This calculation relies on the assumption that the Arabian Sea end member exchanging water with the Gulf of Kutch has a $\Delta^{14}C$ time series generated by our model (using GEOSECS stn 416 $\Delta^{14}C$ for 1977 value as a constraint).

Appendix I

Relative significance of radiocarbon decay term in mass balance equations (3.7).

In this mass balance equations for ^{14}C in the GKh and in the surface layers of the Arabian Sea, we have neglected the radiocarbon decay term.

The ratio of radiocarbon decay in the GKh to its atmospheric flux is

$$\alpha = \lambda \frac{C_G R_G D_G}{F_{12} R_A}$$

considering $R_A \sim R_G$, a minimum value of $F_{12} = 1$ and $C_G D_G \sim 60$ mol m^{-2}, we have $\alpha \sim 10^{-2}$

Similarly the ratio of the radiocarbon decay term in the mixed layer of the Arabian Sea (depth 60m) to its upwelling flux from deep water is

$$\beta = \lambda \frac{C_S R_S D_S}{u C_D R_D}$$

where u is the upwelling velocity. Considering $C_S R_S / C_D R_D \sim 1$ and $D_S/u \sim 10$ we get $\beta \sim 10^{-3}$.

These rough calculations show that the radiocarbon decay is insignificant compared to its supply/removal fluxes in the GKh and in the mixed layer of the Arab. Sea. Therefore it has not been included in our model.

Appendix-II

The no. of mol of $^{14}C (i.e. C^*)$ per unit m^3 of ocean water (Stuiver 1980a) is written as:

$$C^* = m \Sigma CO_2 (1 + \Delta^{14}C/1000)$$

where m is constant which is obtained by multiplying the $^{14}C/^{12}C$ mol ratio in the NBS oxalic acid standard and the fractionation term for transfer of carbon between different

reservoirs.

That is, $m = 1.176 \times 10^{-12} \times 1.052 = 1.24 \times 10^{-12}$

So,

$$\begin{aligned} \frac{dC^*}{dt} &= m\Sigma CO_2 \frac{d}{dt}(1 + \Delta^{14}C/1000) \\ &= \frac{m}{1000}\Sigma CO_2 \frac{d}{dt}\Delta^{14}C \\ &= k\Sigma CO_2 \frac{d}{dt}\Delta^{14}C, [k = \frac{m}{1000}] \end{aligned}$$

Appendix III

Equation for calculating radiocarbon time series in GKh:

Eqn (3) can be written as follows:

$$\frac{d}{dt}\Delta^{14}C_G = \frac{F_{12}}{D_G\Sigma}(\Delta^{14}C_A - \Delta^{14}C_G) + \frac{W}{D_G}(\Delta^{14}C_S - \Delta^{14}C_G)$$

[considering $(\Sigma CO_2)_S = (\Sigma CO_2)_G = \Sigma$]

$$\frac{d}{dt}(\Delta^{14}C_G) + J(\Delta^{14}C_G) = E\Delta^{14}C_A + F\Delta^{14}C_S$$

where,

$$\begin{aligned} E &= \frac{F_{12}}{D_G\Sigma} \\ F &= \frac{W}{D_G} \\ J &= \frac{\frac{F_{12}}{\Sigma} + w}{D_G} = E + F \end{aligned}$$

Appendix IV

Equation for radiocarbon time series in surface Arabian Sea:

Eqn (8) can be rearranged as

$$\frac{d}{dt}\Delta^{14}C_S + \frac{F_{12} + u(\Sigma CO_2)_D}{D_S(\Sigma CO_2)_S}\Delta^{14}C_S = \frac{F_{12}}{D_S(\Sigma CO_2)_S}\Delta^{14}C_A + \frac{u(\Sigma CO_2)_D}{D_S(\Sigma CO_2)_S}\Delta^{14}C_D$$

$$\frac{d\Delta^{14}C_S}{dt} + A(\Delta^{14}C_S) = B(\Delta^{14}C_A) + C$$

where,

$$A = \frac{F_{12} + u(\Sigma CO_2)_D}{D_S(\Sigma CO_2)_S}$$

$$B = \frac{F_{12}}{D_S(\Sigma CO_2)_S}$$

$$C = \frac{u(\Sigma CO_2)_D}{D_S(\Sigma CO_2)_S}\Delta^{14}C_D$$

Appendix-V

If the CO_2 invasion and evasion rates in the Gulf of Kutch are equal then the carbon required for precipitation of coral $CaCO_3$ has to be derived from the incoming water from the Arabian Sea. This requires that the Σ CO_2 of incoming Arabian Sea water to be higher than that of GKh. This contradicts our assumption $[\Sigma\ CO_2]_G$=$[\Sigma\ CO_2]_S$. However as corals covering a very small percentage of the GKh area the difference within Σ CO_2 between these two waters is likely to be very small, hence we neglect the difference for simplifying the calculations.

III.4 Cadmium analysis

The coral KV-1 was chosen for Cd analysis. Its high growth rate enabled subseasonal sampling (5 samples/yr) to investigate seasonal changes in the upwelling characteristics of the Lakshadweep region. The Fig 3.29 shows the variations in Cd concentration in subannual bands. In the first two years of its growth (1984-85) the Cd concentration is < 2 nmol Cd/mol Ca, a typical value for corals growing in upwelling regions. Shen *et al.* (1992) observed that the mean Cd concentration was 2-3 nmol Cd/mol Ca in corals from Galapagos island. But in the next two years our coral shows an anomalous behaviour. Two high peaks are seen in each of these two years. They range from 15 to 22 nmol Cd/mol Ca. The figure also shows the $\delta^{18}O$ (thin line) of this coral, as $\delta^{18}O$ of the corals respond to upwelling. In the first two years there is no significant change in Cd concentration, but in the year 1985 it shows a covariation with $\delta^{18}O$. However in the year 1986 the $\delta^{18}O$ peak and Cd peaks are out of phase. This inconsistency in Cd variations could be due to the coral being young. Similar problems with young corals were also noted by other investigators. Shen (pers. comm., 1993) found abnormally high peaks (≥ 20 nmol Cd/mol Ca) in corals from Champion island and Urvina Bay. Unless the behaviour of young corals with respect to the incorporation of Cd is understood, it is not possible to attach environmental significance to Cd measurements from such corals.

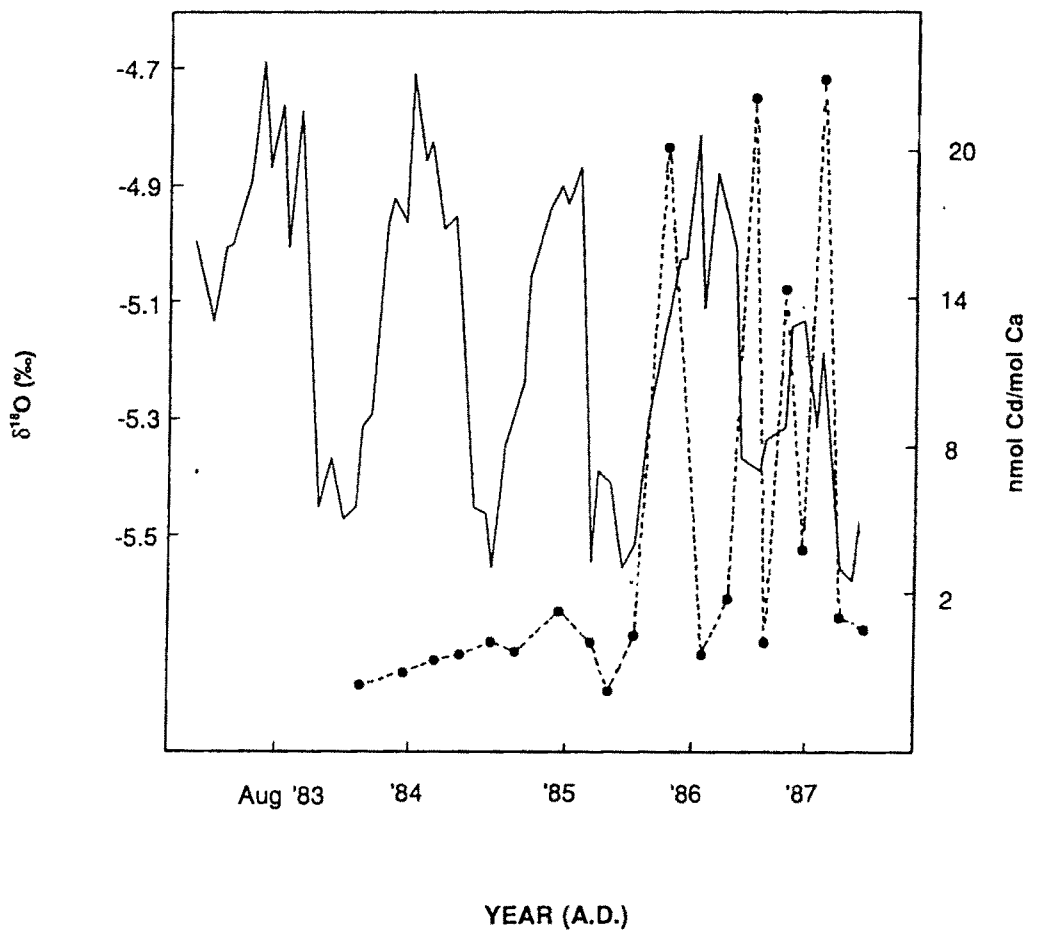

Fig 3.29 The variations of Cd concentration (dotted line) and $\delta^{18}O$ (solid line) in coral *P. compressa* (KV-1) from the Kavaratti lagoon, Lakshadweep islands.

III.5 SYNTHESIS

All the corals analyzed in this thesis are influenced by monsoon systems, the Lakshadweep and the Gulf of Kutch corals by the Indian monsoon and the Stanley Reef coral by the Australian monsoon. Therefore, it would be interesting to compare the isotopic profiles of these samples to look for commonality and the causative factors. However quantitative comparisons are hampered even between the Gulf of Kutch and the Lakshadweep corals (GK & KV2) as the analyses were made on different species, having significantly different growth rates (making it difficult to sample exactly the time contemporaneous sections). Further the SST in these regions is controlled by different factors such as the solar heating (Australia & the Gulf of Kutch) and upwelling (Lakshadweep region). However a qualitative comparison gives the following information:

The oxygen isotope records of the corals (KV2 & GK) from both these locations contain in them monsoon signatures in their oxygen isotopic records in terms of SST and monsoon rainfall respectively. The isotopic profiles of these corals show different trends. This arises because of the different factors which determine the SST in these two regions. The Lakshadweep region is more affected by monsoon induced upwelling and hence sea surface cooling with a minimum SST around Jul-Aug. The coral (*Porites*) from this region accurately records the sea surface temperature variations in their oxygen isotopic ratios registering a maximum in Jul-Aug. The Gulf of Kutch is less influenced by upwelling compared to Lakshadweep region. Here the magnitude of variation in SST is much higher (~6 °C) than in Lakshadweep (~3 to 4°C). The large variation is brought about by summer heating and winter cooling. The lower SST is during Dec-Jan while in Lakshadweep it is in Jul-Aug. The slow growth rate of the GK coral also places a constraint in quantitatively determining the amplitude of seasonal $\delta^{18}O$ variation. The $\delta^{18}O$ of this coral (GK) also shows an apparent higher order cyclicity.

When we compare the SR coral and Lakshadweep coral (they are of the same genus), we find that the $\delta^{18}O$ time series and growth rates are similar. They show a very good resemblance in their oxygen isotopic distributions. The mean $\delta^{18}O$ of these two corals are -5.07 ± 0.36 and -5.16 ± 0.21 respectively. The mean amplitudes are 0.75 ± 0.1 and

0.55±0.19, corresponding to ~5°C and ~3 °C seasonal SST fluctuation respectively. The SR region shows an SST minimum during Austral winter(Jul-Aug) and maximum in summer (Dec-Jan). In case of Lakshadweep the minimum temperature is registered at the same time, Jul-Aug while maximum is around Apr-May. For this reason the $\delta^{18}O$ maxima in these two corals coincide while the minima are phase shifted.

Another interesting feature is the $\delta^{13}C$ values of these two corals are 180° out of phase. This contrasting behaviour in the $\delta^{13}C$ can be explained as follows:

The coral $\delta^{13}C$ is to some extent controlled by the rate of photosynthesis, which depends on the availability of sunlight. More cloudiness reduces availability of sunlight and hence the photosynthesis rate. This would result in lower $\delta^{13}C$ value. The cloudiness in the Lakshadweep region is maximum during the monsoon period, Jun-Sep when $\delta^{13}C$ shows a reduction. During the same period the SR region experiences a relatively cloudfree winter, contributing to a rising trend in the coral $\delta^{13}C$. The long term decreasing trend in both the cases are also remarkably similar. Further investigations on this aspect may be helpful in relating the southwest Indian monsoon and the Australian monsoon, the individual components of the broad-scale Asian monsoon.